Study of Thrust Conversion Process of Explosive Plasma Source in Dipole Magnetic Field by Using Three - Dimensional Hybrid Code

VCHIVKOV Konstantin

Study of Thrust Conversion Process of Explosive Plasma Source in Dipole Magnetic Field by Using Three - Dimensional Hybrid Code

K.V. Vchivkov

ABSTRACT

A magnetic thrust chamber using a dipole magnetic field can control the plasma flow resulting from explosive plasma sources such as laser thermal propulsion and inertial confinement fusion rockets. The chamber has advantage in that its thermalization with the wall structures of the chamber can be avoided.

The main goal of the present study has been investigation of thrust conversion process in the magnetic thrust chamber by using a $3D$ hybrid Particles - In - Cells (PIC) code. The study is crucial for designing optimal configuration of the magnetic thrust chamber.

Chapter 1 contains a general introduction of computer simulation for plasma physics problems and background of the present study. Chapter 2 reviews the main equations and methods that are used in the $3D$ hybrid PIC code. A brief description of the main cycle of the code is given. Chapter 3 is devoted to the study on the thrust conversion processes in the magnetic thrust chamber by using comparative analysis of laser - produced plasma experiment and PIC simulation. A study on optimization of thrust efficiency in the chamber by using the $3D$ hybrid PIC code is presented in Chapter 4. A numerical analysis is performed in Chapter 5 for the direct conversion of the plasma clouds energy into electrical energy during the expansion in a magnetic field. Finally, Chapter 6 contains conclusions and suggestions for the future work.

To investigate the plasma behavior and thrust conversion process in the magnetic thrust chamber, we make a comparison analysis of laser - produced plasma experiment and PIC - simulation in a scaled - down model. The temporal evolutions of

laser - produced plasma cloud (LPC) expanding in the dipole magnetic field and the magnetic field disturbances ΔB caused by the diamagnetic cavity of plasma are examined and the thrust conversion efficiency is estimated. An overall qualitative agreement between experimental and simulation data is found.

We optimize the thrust efficiency by the approach that is based on the analysis of retardation model of plasma cloud expansion. The model shows a cone - like geometry. Half angle of the plasma expansion cone α is estimated. Overall qualitative agreement is found between the simulation and the theoretical model of Nikitin for dependences of the thrust efficiency η on α and energetic criterion κ. From the obtained simulation results the maximum thrust efficiency is about 70%, however in the MHD theoretical work the efficiency reaches about 85%.

In the magnetic thrust chamber, some part of initial plasma energy could be directly transferred into electric energy by the magnetic field disturbance. We have studied the conversion process by comparison analysis between experiment and simulation. The direct energy conversion is realized due to inductive generation of currents in a pickup coil that encloses the plasma. It has been shown that in the experimental result there is the flute instability, but we do not observe the instability in the simulation results. A reasonable agreement is found for dependence of the gap size δ on the similarity criterion of the problem β. The experimental value of conversion efficiency is $4.5 \pm 0.9\%$, while from the simulation results the efficiency is estimated to be 7.9%. To decrease the difference, more sophisticated model with the instability term is required for the model of induced pickup coil current.

In summary, the behaviors of explosive plasmas in the magnetic thrust chamber are analyzed by the $3D$ hybrid PIC code developed here. Simulation results are compared with the experimental ones, and overall qualitative agreement is obtained, thus validating the usage of the $3D$ hybrid code in simulating the thrust conversion process in the chamber. From optimization study to maximize the thrust efficiency, the code suggests that a thrust efficiency as high as 70% would be possible in the

chamber. These facts would support the assumptions made in the chamber design and would also substantiate the idea of direct and highly effective usage of explosive plasma sources in the form of magnetic thrust chamber for propulsion purposes.

Contents

1 Introduction

1.1 Computer simulation for plasma physics problems

Study of plasma behaviors is very necessary for understanding the physics phenomena of cosmic and laboratory plasmas. Examples of such physics phenomena are expansion of laser produced plasma cloud into an ambient magnetic field in fusion reactor, supernova explosion, interaction of the solar wind with planets magnetosphere and with artificial objects and phenomena that are observed in cosmic and laboratory experiments.

It is difficult and sometimes impossible to obtain enough information about plasma phenomena from experiments, and therefore computer simulation is a very useful method for investigations. The computer simulation methods for plasma physics were developed from a progress and requirements of the works which are related to the controlled fusion and cosmic space investigations. The progress of new computer generations also contributed to the evolution of the methods.

The main foundations of computational plasma physics were created by A.A. Samarskii, N.N. Yanenko, A.B. Langdon, B.F. Lasinski, J. Villasenor, O. Buneman and their colleagues and scientists.

Fundamental stage of the computer simulation is a construction of numerical model. An original problem is formulated by using differential equations and the necessary transfer from the original problem to a discrete algebraic approximation is realized. The discrete algebraic equations describe the numerical model which, when expressed as a sequence of computer instructions, provides the simulation code. The computer code then allows the evolution of the model physical system to be investigated in computer experiment.

Choice of the discretization method substantially influences the numerical model, further composition of the algorithm and architecture of a corresponding simulation code. The best known discretization method is a method which uses finite - difference approximations of the differential equations, i.e. finite - difference methods

and schemes.

In this thesis for problems of plasma expansion into ambient magnetic field in magnetic thrust chamber scheme of plasma propulsion such as laser fusion rocket (LFR) we use a set of equations consisting of Vlasov's kinetic equations for the distribution functions of the ions and electrons and a set of Maxwell equations. The densities of current and charge involved in the Maxwell equation are calculated from the distribution functions of the ions and electrons. The Vlasov's equations are solved by particles in cells (PIC) method and Maxwell equations by finite - difference methods on uniform rectangular grid.

The PIC method is at present the most universal and much used method for solving the physical problems in collisionless plasma. The method reduces the problem of solving the particles motion equation in a 6-dimensional (three spatial variables and three components of velocity) space to the problem of integrating the equation of motion for individual particles.

Feature of PIC method is a concept of the transfer from the original problem to the discrete approximation. The concept is as follows: the plasma is simulated by the finite set of the discrete particles (each of which symbolizes an action of many physical particles). Each particle has characteristics such as mass, electrical charge, velocity, kinetic energy and spatial coordinates. The state of the physical system is defined by the attributes of a finite ensemble of particles and the evolution of the system is determined by the laws of interaction of the particles. The fundamental laws which control the plasma behavior are as follows: the charged particles move in accordance with the laws of classical mechanics in a self - consistent electromagnetic field.

A feature which makes particle model computationally attractive is that a part of the particle attributes is conserved quantity and so need no updating as the computer simulation evolves in time [1].

For finding electrical and magnetic field we use a scheme which was offered by

A. Langdon and B. Lasinski in 1976 [2]. In the scheme, fields are defined from the finite - difference version of Faraday's and Ampere's laws. In this scheme, the values of components of the intensity of electric and magnetic fields are computed in the nodes of grids, which are shifted relative to each other with respect to time and space.

Many studies are dedicated to the numerical analysis of plasma behavior under an ambient magnetic field. For instance, Harned [3] uses a hybrid algorithm which treats ions as particles and electrons as an inertialess fluid. The Darwin limit of Maxwell's equations (i.e., neglecting the transverse displacement current) is used. The electron momentum equation, with inertial terms neglected, is coupled with Maxwell's equations and the statement of quasineutrality in order to determine the electric and magnetic fields. In the paper the author described a two - dimensional quasineutral model.

Horowitz et al. presented [4] a PIC model in Cartesian coordinates. The model is implemented in a FORTRAN code. The major elements of this code are presented including the many techniques required for its optimization. The authors discuss many of the major factors in optimization that are dependent upon features of the Cray-2 multiprocessor. Results of the code testing are presented.

1.2 Background of the present study

An analysis of plasma behavior in a dipole magnetic field, especially for the case where explosive plasma source locates near its pole is very useful to design plasma propulsion systems such as inertial confinement fusion rockets and laser thermal propulsion [5]. Here, we will take up LFR as a concrete example for further discussions, although the results obtained are applicable to other systems mentioned above.

A high performance rocket must have both a large exhaust velocity and a low mass of power plant [6]. The nuclear fuel makes it energetically feasible to eject propellant with high exhaust velocity. By burning this fuel explosively, production of energy and thrust can be substantially decoupled from the vehicle. Thus, the rocket could operate with a high power - to - mass ratio, combining its fuel - efficient high exhaust velocity with the acceleration required for short trip times.

By the starts of the 1970's, progress in high power laser led to initiation of programs to develop inertial confinement fusion (ICF) for terrestrial powerplants. It also led to renewed interest in laser fusion rockets (LFR) which used ICF micro - explosions. The concepts of LFR design were presented in Ref. [6]. In these concepts, a fusion pellet is exploded within a magnetic nozzle, i.e. a magnetic thrust chamber. As the resultant pellet debris expands, it is controlled by magnetic fields and expelled from the thrust chamber. This produces thrust, while preventing the pellet debris from physically hitting the rocket.

According to Hyde's concepts [6], LFR consists of three major systems: the fusion pellet, the "Driver" which implodes and ignites it and the thrust chamber that uses the micro - explosion to produce thrust. The author discussed the principles of these systems and some of the options available in the design of an interplanetary LFR.

In Refs. [7] and [8] a new vehicle concept called Vehicle for Interplanetary Space Transport Applications ($VISTA$) is developed (Fig. 1.1). The authors describe

VISTA's engine operation, discuss associated plasma issues and describe the advantages of *DT* fuel for near term applications.

VISTA has a 6% - efficient excimer-laser driver operating at $1000\,K$ with an output of $5\,MJ$, and uses pellets that allow energy gains from 200 up to perhaps 1500. Its effective specific impulse is about $17,000\,s$, with a thrust efficiency near 60% . When operating at a maximum pellet repetition rate of $30\,Hz$, VISTA's power system has a power-to-mass ratio near $20\,W/g$, a mass flow rate of $1.5\,kg/s$, a thrust of $2.4 \times 10^5\,N$, and a jet power of $2.0 \times 10^4\,MW$.

VISTA's overall geometry is that of a 50° half-angle cone. This shape is required to avoid massive radioactive shielding and to keep fusion neutrons (and x - rays) from striking and heating vehicle surfaces. The 50° half angle maximizes the thrust efficiency, and is determined by selecting the optimum pellet firing position along the axis of the cone with respect to the plane of the magnetic coil, in a manner similar to that was carried out by Hyde [6]. The magnetic coil is located at the bottom of the spacecraft and the pellet is positioned at the apex of the cone, with two final laser focusing mirrors being used to irradiate the pellet.

1.3 Aim of this study

The aims of the present study are as follows.

— To examine the thrust conversion process in a magnetic thrust chamber for a scaled-down model by comparing the experimental work with our simulation results. The expansion of laser - produced plasma cloud in the dipole field is studied under the conditions close to LFR magnetic thrust chamber. The results of simulation studies are obtained by using a 3D hybrid code and the plasma behavior in the chamber is examined.

— To optimize the thrust efficiency by investigating the dependences of half angle of plasma expansion cone α on the energetic interaction parameter κ (the parameter characterizes the interaction between the expanding plasma and the dipole field) and of the thrust efficiency η on the cone angle α.

— To conduct a numerical analysis on the direct conversion of the plasma clouds energy into electrical energy during the expansion in a magnetic field. For the purpose the $3D$ hybrid PIC code is used. In this study we are comparing the efficiency of such a conversion process between experiment and simulation.

1.4 Structure of this thesis

The structure of this thesis is as follows.

Chapter 1 contains a general introduction of computer simulation for plasma physics problems and background of the present study.

Chapter 2 reviews the main equations and methods that is used in the $3D$ hybrid PIC code. A brief description of the main cycle of the code is given.

Chapter 3 is devoted to the study on the thrust conversion processes in the magnetic thrust chamber by using comparative analysis between laser - produced plasma experiment and PIC simulation.

A study on optimization of thrust efficiency in the magnetic thrust chamber by using the $3D$ hybrid PIC code is presented in Chapter 4.

A numerical analysis is performed in Chapter 5 for the direct conversion of the plasma clouds energy into electrical energy during the expansion in a magnetic field.

Finally, Chapter 6 contains conclusions and suggestions for the future work.

References

[1] HOCKNEY R.W. AND EASTWOOD J.W.: "COMPUTER SIMULATION USING PARTICLES", *Adam Hilger, Bristol and Philadelphia,* (1988).

[2] LANGDON A.B. AND LASINSKI B.F: *Meth. Comput. Phys.,* **16** (1976) 327.

[3] HARNED D.S.: *J. of Comp. Phys.,* **47** (1982) 452.

[4] HOROWITZ E.J., SHUMAKER D.E. AND ANDERSON D.V.: *J. of Comp. Phys.,* **84** (1988) 279.

[5] ARAKAWA Y. AND YOSHIKAWA K.: *Space power,* **7** (1998) 17.

[6] HYDE R.A.: UCRL-88857, *Lawrence Berkeley Laboratory,* (1983).

[7] ORTH C.D., KLEIN G., SERCEL J., HOFFMAN N., MURRAY K., CHANG-DIAZ F.: AIAA-87-1904, (1987).

[8] ORTH C.D., KLEIN G., SERCEL J., HOFFMAN N., MURRAY K., CHANG-DIAZ F.: UCRL-96676, (1987).

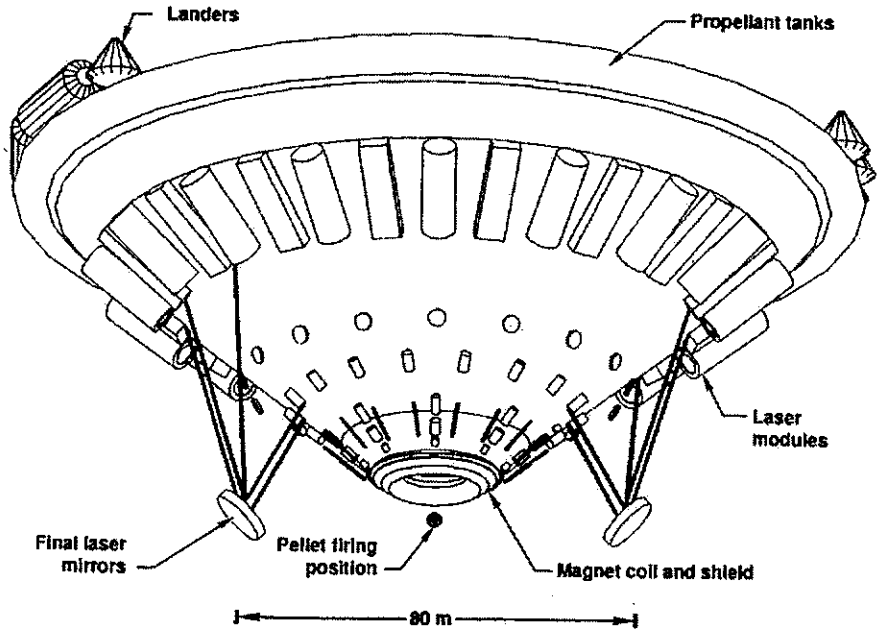

Fig. 1.1 *VISTA* system layout.

2 Numerical model

2.1 Introduction

Generally, the appropriate original model of collisionless plasma is the equations system, which consists of kinetic Vlasov's equations:

$$\begin{gathered}\frac{\partial f_{i,e}}{\partial t}+\vec{v}\frac{\partial f_{i,e}}{\partial \vec{r}}+\vec{F}_{i,e}\frac{1}{m}\frac{\partial f_{i,e}}{\partial \vec{v}}=0,\\ \vec{F}_{i,e}=q_{i,e}\left(\vec{E}+\vec{v}\times\vec{B}\right).\end{gathered} \tag{2.1}$$

and a system of Maxwell's equations:

$$\nabla\times\vec{B}=\mu_0\vec{J}+\frac{1}{c^2}\frac{\partial\vec{E}}{\partial t}, \tag{2.2}$$

$$\nabla\times\vec{E}=-\frac{\partial\vec{B}}{\partial t}, \tag{2.3}$$

$$\nabla\left(\epsilon_0\vec{E}\right)=\rho, \tag{2.4}$$

$$\nabla\vec{B}=0. \tag{2.5}$$

The densities of current and charge involved in the Maxwell equations are calculated from the distribution functions of the ions and electrons by using the following formulas:

$$\vec{J}=\sum_{i,e}q_{i,e}\int f_{i,e}\vec{v}\,d\vec{v},$$

$$\rho=\sum_{i,e}q_{i,e}\int f_{i,e}\,d\vec{v}.$$

Here, indexes i and e indicate a kind of particles (i for ions and e for electrons), $f_{i,e}$ is the distribution function of the ions and electrons, $f_{i,e}\equiv f_{i,e}(\vec{r},\vec{v},t)$ ($\vec{r}$, $\vec{v}$ and t are the vector of particles positions, vector of particles velocities and time, respectively), $q_{i,e}$ the particle charge, m the particle mass, $\vec{J}$ the current density, ρ the density of spatial charge, ϵ_0 the free - space permittivity and μ_0 the vacuum magnetic permeability. $\vec{E}$ and $\vec{B}$ are the intensities of electric and magnetic fields, respectively.

It follows that for solving the physical problems we have a complex differential equation system for the ions and electrons distribution functions of the coordinates and velocities. The Vlasov's equations are the equations of seven arguments (time, three spatial variables and three components of velocity) and Maxwell equations are the equations for the functions of four arguments (time and three spatial variables).

After specifying initial and boundary conditions on the base of the above mentioned equations a nonstationary problem is formulated in 6 - dimensional space of coordinates and velocities.

From the mathematical standpoint the Vlasov equation is an equation of hyperbolic type, which can be written in Euler or Lagrangian coordinates [1], [2]. These two terms were adopted from hydrodynamics [3].

In Euler coordinates the plasma characteristics are functions that are defined in a coordinate system which is fixed on space. When the Euler coordinates are applied, the usage of finite - difference schemes is appropriate for the problem. In the schemes the values of grid functions that are defined at nearby nodes of introduced grid system are connected with each other by the approximation of derivatives.

The approach that is related to the name of Lagrange is as follows: the plasma is considered as a set of particles. Then any evolution characteristics of the plasma are defined as trajectories of the particles. In 6 - dimensional space, when the Lagrangian coordinates are used, it is also possible to introduce a spatial grid system at the nodes of which values of the functions are given. Thus, the coordinates of nodes are connected with plasma moving, that usually is a serious disadvantage, when the equations are solved by finite - difference methods, because in the course of solution there occurs a deformation of the Lagrangian grid. And this renders the approximation of spatial derivatives impossible.

The Vlasov equation in Lagrangian coordinates becomes as follows:

$$df/dt = 0,$$

i.e, there are no space and velocities derivatives in the equation. Its solution indi-

cates that the value of the distribution function is not changed in motion along the characteristic curve of equation and does not depend on the values of the distribution functions in other points of space.

The characteristic equations are as follows:

$$\frac{d\vec{r}}{dt} = \vec{v},$$

$$\frac{d\vec{v}}{dt} = \frac{1}{m}\vec{F}.$$

In PIC method the characteristic equations define the paths of the plasma particles.

The plan of this chapter is as follows. In Section **2.2** we discuss our calculation model and assumptions adopted here. Section **2.3** describes PIC method. The method is used for solving Vlasov's equation. Method of solving Maxwell's equations is presented in Section **2.4**. The main subroutines and computational cycle of three - dimensional ($3D$) PIC hybrid code are described in Section **2.5**. The conclusions are given in Section **2.6**.

2.2 Basic equations and assumptions

To calculate the plasma behavior under the dipole magnetic field we have developed a $3D$ hybrid PIC code based on the model given by Harned [4] and Horowitz et al. [5]. The hybrid code treats ions as individual particles and electrons as a fluid. This approach is valid when the system behavior is dominated by ion physics.

The equations controlling our system can be derived from Maxwell's equations and the equations of motion of particles. The basic equations of the model are as follows.

The electric field is computed from the momentum equation for an electron fluid

$$n_e m_e \left(\frac{d\vec{v}_e}{dt}\right) = -en_e\left(\vec{E} + \vec{v}_e \times \vec{B}\right) - \nabla P_e, \tag{2.6}$$

where m_e is the electron mass, n_e the electron density, e the elementary electric charge, $\vec{v}_e$ the electron velocity, $\vec{E}$ the electric field and $\vec{B}$ the total magnetic field.

P_e is the electron pressure given by

$$P_e = n_e T_e, \tag{2.7}$$

where T_e is the electron temperature and is assumed to be uniform for simplicity.

The electrons are approximated as a massless fluid, so the left-hand side of (2.6) becomes zero and

$$\vec{E} = -\vec{v}_e \times \vec{B} - \frac{1}{en_e}\nabla P_e. \tag{2.8}$$

Ampere's law with Darwin approximation, which indicates that high-frequency electromagnetic waves do not exist, reduces to

$$\nabla \times \vec{B}_p = \mu_0 \left(\vec{J}_e + \vec{J}_i\right), \tag{2.9}$$

where $\vec{B}_p$ is the magnetic field generated by plasma current density and it is evaluated from the equation $\vec{B}_p = \vec{B} - \vec{B}_{ext}$, where again $\vec{B}_{ext}$ is the external magnetic field. Substituting $-en_e\vec{v}_e$ for J_e in Ampere's law, solving for $\vec{v}_e$, and substituting the $\vec{v}_e$ into (2.8), we obtain

$$\begin{aligned}\vec{E} = \frac{1}{\mu_0 Z e n_i}\left(\nabla \times \vec{B}_p\right) \times \vec{B} - \frac{1}{Z e n_i}\vec{J}_i \times \\ \times \vec{B} - \frac{T_e}{en_i}\nabla n_i.\end{aligned} \tag{2.10}$$

We assume quasi-neutrality and set the ion charge density equal to the electron charge density, i.e.,

$$Z n_i = n_e \tag{2.11}$$

in equation (2.10), where Z is the charge state of the ion. Equation (2.10) includes the terms inversely proportional to the ion density n_i. In a vacuum region, these terms must cause numerical infinity. We solve the Laplace equation to obtain the electric field in a vacuum region,

$$\nabla^2 \vec{E} = 0. \tag{2.12}$$

Ion density n_i and current density J_i are calculated by the PIC method based on particle position $\vec{r}_i$ and velocity $\vec{v}_i$ which are obtained by integrating the equations

of motion given as

$$\frac{d\vec{v}_i}{dt} = \frac{Ze}{m_i}\left(\vec{E} + \vec{v}_i \times \vec{B}\right), \tag{2.13}$$

$$\frac{d\vec{r}_i}{dt} = \vec{v}_i. \tag{2.14}$$

where m_i is the mass, Ze the charge, $\vec{v}_i$ the velocity and $\vec{r}_i$ the position of the ion.

The magnetic field is advanced by Faraday's law

$$\frac{\partial \vec{B}}{\partial t} = -\nabla \times \vec{E}. \tag{2.15}$$

Cartesian coordinates (X, Y, Z) are adopted here. The time levels of the ion position and field quantities are defined at an integer time step, and the ion velocity and current density at a half-time step. The leapfrog method which is a time-centered difference scheme is adopted to solve the ion's equations of motion. Faraday's law is solved using the backward difference scheme in time. Field quantities, ion density and current density are spatially defined at the same grid points.

The boundary condition adopted here for the field quantities is that the spatial differences of the normal components are set to be zero at the surface of the cylindrical calculation region.

The initial distributions of the particle positions and velocities are assumed to be uniform. The initial plasma location is the same as in the experiment.

2.3 Method of solving particles motion equations

On the base of the description of Vlasov equation in Lagrangian variable the *PIC* method is developed.

As was explained in Chapter **1**, in this method the entire plasma is simulated by the set of discrete particles. Characteristics of Vlasov equation (2.1) describe the paths of these particles. The amount of chosen particles is determined by the necessary accuracy of solution and available computer resources (memory and speed). It follows that the *PIC* method reduces the problem of solving the Vlasov equation

in a 6 - dimensional space to the problem of integrating the equations of motion for individual particles.

In this thesis, for equations (2.13) and (2.14) we use the scheme as follows:

$$\begin{gathered}\frac{\vec{v}_i^{\,n+1/2}-\vec{v}_i^{\,n-1/2}}{\Delta t}=\frac{Ze}{m_i}\left\{\vec{E}^n+\frac{1}{2}\left(\vec{v}_i^{\,n+1/2}+\vec{v}_i^{\,n-1/2}\right)\times\vec{B}^n\right\},\\ \frac{\vec{r}_i^{\,n+1}-\vec{r}_i^{\,n}}{\Delta t}=\vec{v}_i^{\,n+1/2}.\end{gathered}\tag{2.16}$$

Here Δt is the time step, index n indicates the moment of time, in which the desired function is calculated. The coordinates of the particles are calculated at $t^n = n\Delta t$ and velocities are calculated at $t^{n+1/2} = (n + 1/2)\,\Delta t$. The scheme is called as *leapfrog scheme*. It is a time-centered difference scheme, therefore it is second order accurate in time.

Model particles are moving along the same trajectories and with the same velocities as the real ions and electrons. Number of the model particles in the small volume, as in the real plasma, determines the density of these particles. Therefore the properties of real and model plasmas are similar. However, some features of the model plasma change greatly from the real plasma. For instance, the length of the free path in the model plasma is much less, but the frequency of collisions is much greater than in the real plasma [1], [6]. Model plasma has a very high level of heat noise. For the elimination of these defects particles of finite size are used in the method.

PIC method has another important technological property such that the particles moving in each cell depend only on the values of electrical and magnetic fields in this cell and do not depend on coordinates and velocities of other particles. Therefore such cells together with the particles in them can be considered independently. The fact allows to easily modify a code, which realizes the *PIC* method, for solving another problems. Only geometrical model, initial and boundary conditions and solving Maxwell equations must be changed. Particles motion inside the cells obeys common laws, independent of problems [2].

Independence of particles motion permits parallel algorithms for solving the particles motion equation and calculations of density of plasma and average velocities of particles. Parallel algorithms give an opportunity to use modern multiprocessor computers for essential reduction of the time of solving the tasks. This, in turn, makes it possible to enlarge the amount of model particles and thus raise accuracy of calculations, hence more fine research of physical processes can be achieved [7].

2.4 Method of solving fields equations

The time advance of field quantities given by equations (2.10) and (2.15) is accomplished by a predictor - corrector algorithm ([4], [5]). If the quantities $\vec{J}_i^{\,n+1/2}$, $\vec{v}_i^{\,n+1/2}$, $n_i^{\,n+1/2}$, $\vec{B}^{\,n}$ and $\vec{E}^{\,n}$ are known, the magnetic field is advanced by

$$\vec{B}^{\,n+1/2} = \vec{B}^{\,n} - \frac{\Delta t}{2}\nabla \times \vec{E}^{\,n} \tag{2.17}$$

and the electric field is calculated as follows:

$$\vec{E}^{\,n+1/2} = \frac{1}{n_i}\left\{\frac{1}{\mu_0 Ze}\left(\nabla \times \vec{B}_p^{\,n+1/2}\right) \times \vec{B}^{\,n+1/2} - \frac{1}{Ze}\vec{J}_i^{\,n+1/2} \times \right. \\ \left. \times \vec{B}^{\,n+1/2} - \frac{T_e}{e}\nabla n_i^{n+1/2}\right\}. \tag{2.18}$$

A prediction is then made for $\vec{E}^{\,n+1}$ and $\vec{B}^{\,n+1}$ by

$$\vec{E}_{pred}^{\,n+1} = -\vec{E}^{\,n} + 2\vec{E}^{\,n+1/2}, \tag{2.19}$$

$$\vec{B}_{pred}^{\,n+1} = \vec{B}^{\,n+1/2} - \frac{\Delta t}{2}\nabla \times \vec{E}_{pred}^{\,n+1}. \tag{2.20}$$

Using the predicted fields, a predictor particle move is performed to obtain $n_{i,pred}^{n+3/2}$ and $J_{i,pred}^{n+3/2}$ after which $\vec{B}_{pred}^{n+3/2}$ and $\vec{E}_{pred}^{n+3/2}$ are predicted by

$$\vec{B}_{pred}^{\,n+3/2} = \vec{B}_{pred}^{\,n+1} - \frac{\Delta t}{2}\nabla \times \vec{E}_{pred}^{\,n+1}, \tag{2.21}$$

$$\vec{E}_{pred}^{\,n+3/2} = \frac{1}{n_i}\left\{\frac{1}{\mu_0 Ze}\left(\nabla \times \vec{B}_p^{\,n+3/2}\right) \times \vec{B}_{pred}^{\,n+3/2} - \frac{1}{Ze}\vec{J}_{i,pred}^{\,n+3/2} \times \right. \\ \left. \times \vec{B}_{pred}^{\,n+3/2} - \frac{T_e}{e}\nabla n_{i,pred}^{n+3/2}\right\}. \tag{2.22}$$

Finally, the new electric and magnetic fields are obtained from

$$\vec{E}^{\,n+1} = \frac{1}{2}\vec{E}^{\,n+1/2} + \frac{1}{2}\vec{E}_{pred}^{\,n+3/2}, \tag{2.23}$$

$$\vec{B}^{\,n+1} = \vec{B}^{\,n+1/2} - \frac{\Delta t}{2}\nabla \times \vec{E}^{\,n+1}. \tag{2.24}$$

The particle position can now be advanced to $n + 3/2$ using these new field quantities. The electric and magnetic fields are stored on different grids.

The predictor - corrector algorithm is second order accurate in time and space. The time step is limited by a Courant - Friedrichs - Lewy (CFL) condition $\Delta t < h/V_0$, where h is the mesh size and V_0 the initial velocity of the particles. An additional constraint on the time step for numerical stability is $\omega_{ci}\Delta t < 2$, where ω_{ci} is the ion cyclotron frequency; however, in practice the CFL condition is the more restrictive requirement.

2.5 Computational cycle of $3D$ PIC hybrid code

In this section we will discuss the main subroutines and computational cycle of $3D$ PIC hybrid code.

The $3D$ hybrid PIC code is designed to calculate the plasma behavior under the dipole magnetic field in fusion reactor.

The code was created by using $FORTRAN77/90$ for $UNIX$ operation system.

2.5.1 Module structure of $3D$ PIC hybrid code

The calculation flow chart for the $3D$ PIC hybrid code is shown in Fig. 2.1.

The subroutines of the part 1 "Initial preparation of 3D hybrid code" shown in Fig. 2.1 perform the following functions:

— read the initial data;

— normalize variables;

— set the initial values of the external magnetic field components;

— calculate the initial values of particle velocities;

— calculate the initial values of current density components;

— calculate the initial particles distribution.

The subroutine in the box 2.1 in Fig. 2.1 calculates the quantities of the electric and magnetic fields at $n+1/2$ time step as explained in Section 2.4 by using equations (2.17) and (2.18).

Then, the next subroutine (box 2.2, Fig. 2.1) makes a prediction for quantities

of the fields $\vec{E}$ and $\vec{B}$ at $n+1$ time step, by using equations of (2.19) and (2.20) of Section 2.4.

The subroutine in box 2.3 in Fig. 2.1 "Predict the particle motion" performs the predictor particles move as follows. The predicted quantities of particles velocities are evaluated by using the predicted quantities of electric $\vec{E}_{pred}^{n+1}$ and magnetic $\vec{B}_{pred}^{n+1}$ fields. Then the particle position and current density are defined as follows:

$$\vec{r}_{pred}^{\,n+3/2} = \vec{r}^{\,n+1} + \frac{\Delta t}{2}\vec{v}_{pred}^{\,n+3/2},$$

$$\vec{J}_{pred}^{\,n+3/2} = Zen_i^{\,n+3/2}\vec{v}_{pred}^{\,n+3/2}.$$

Subroutine in box 2.4 in Fig. 2.1. predicts the quantities of $\vec{B}_{pred}^{n+3/2}$ and $\vec{E}_{pred}^{n+3/2}$ by using equations (2.21) and (2.22) of Section 2.4.

The final quantities of $\vec{E}^{\,n+1}$ and $\vec{B}^{\,n+1}$ are calculated by equations (2.23) and (2.24) of Section 2.4 (see box 2.5, Fig. 2.1).

In the box 2.6 in Fig. 2.1 the particle positions and current at time step $n+3/2$ are calculated as follows:

$$\vec{r}^{\,n+3/2} = \vec{r}^{\,n+1} + \frac{\Delta t}{2}\vec{v}^{\,n+3/2},$$

$$\vec{J}^{\,n+3/2} = Zen_i^{\,n+3/2}\vec{v}^{\,n+3/2}.$$

We continue to iterate until successive iterations give the same result to within some predetermined error tolerance ε:

$$\frac{max_{i,j,k}\left|B_{i,j,k}^{n+1\ (iter+1)} - B_{i,j,k}^{n+1\ (iter)}\right|}{max_{i,j,k}\left|B_{i,j,k}^{n+1\ (iter)}\right|} \leq \varepsilon,$$

where $(iter)$ is the number of the iteration.

The subroutine in the box 3 in Fig. 2.1 saves the calculation data for future treatment or continuation of the calculation.

2.6 Conclusions

In this chapter we described a numerical model that was adopted to the problem of plasma expansion into ambient magnetic field in magnetic nozzle scheme of LFR. We use a set of equations consisting of Vlasov's kinetic equation for the distribution functions of the ions and electrons and a set of Maxwell equation.

In the plasma there are quite different time scales of electrons and ions motion. The fact complicates the simulation of plasma physics problems. For instance, if we are interested in the ions motion, then we should also consider the electrons motion. The velocity of electrons is faster than that of ions. Since, according to the CFL condition, the time step in nonstationary problems should not exceed h/V_0, then we are forced to make a calculation with small, relative to ions, time step. For overcoming this disadvantage we will use the hybrid model. In the model ions are treated as individual particles and electrons as fluid.

The Maxwell equations are solved by finite - difference methods on uniform rectangular grid and the Vlasov's equations by PIC method.

The problems that arise in the plasma physics is usually two or three dimensional, consequently ions distribution function depends on many variables such as time, coordinates and velocities. Taking into account this fact, we will use PIC method because the method reduces the problem of solving the particles motion equation in a 6 - dimensional space to the problem of integrating the motion equation for individual particles.

References

[1] TAJIMA T.: "Computational plasma physics: with applications to fusion and astrophysics", *Addison - Wesley Publishing Company, Inc.,* (1989).

[2] GRIGORYEV YU.N., VSHIVKOV V.A. AND FEDORUK M.F.: "Numerical particle-in-cell methods: theory and applications", *Utrecht; Boston : VSP,* (2002).

[3] KOCHIN N.E., KIBEL I.A. AND ROZE N.V.: "Theoretical hydrodynamics", *M: FM,* **Part 1** (1963) [in Russian].

[4] HARNED S.D.: *J. Comp. Phys.,* **47** (1982) 452.

[5] HOROWITZ E.J., SHUMAKER D.E. AND ANDERSON D.V.: *J. Comp. Phys.,* **84** (1989) 279.

[6] HOCKNEY R.W. AND EASTWOOD J.W.: "COMPUTER SIMULATION USING PARTICLES", *Adam Hilger, Bristol and Philadelphia,* (1988).

[7] VSHIVKOV V.A., VCHIVKOV K.V. AND DUDNIKOVA G.I.: *J. Comp. Tech.,* **46** No.2 (2001) 47 [in Russian].

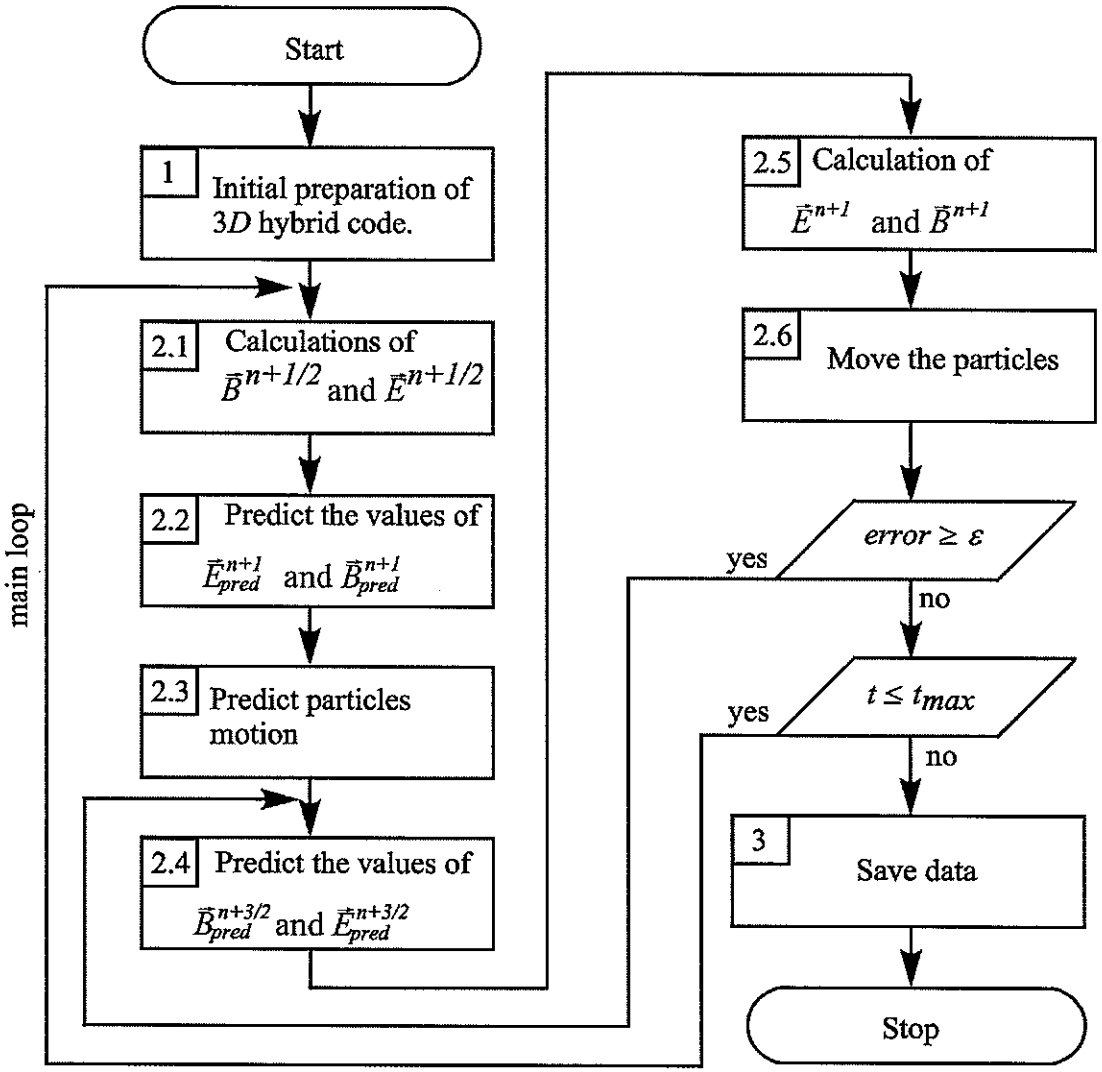

Fig. 2.1 Flow chart of $3D$ hybrid code.

3 Study on thrust conversion process in magnetic thrust chamber by using comparative analysis of laser - produced plasma experiment and PIC simulation

3.1 Introduction

Here, we discuss the thrust conversion process in a dipole magnetic field putting emphasis on a thrust chamber of LFR to make the discussions more clear.

LFR is an innovative idea proposed by Hyde [1]. A fusion reaction can release a large amount of energy and easily produce plasma of high temperature and density. The resulting plasma flow can be controlled by a properly designed applied magnetic field geometry, i.e., a magnetic thrust chamber. In the laser fusion rocket, the chamber is composed of a solenoidal superconducting coil.

The fusion reaction occurs by irradiation of a laser onto a fuel pellet and the resulting plasma expands isotropically at an early stage. The plasma is a good conductor, so when a magnetic field is applied, the plasma particles move around the magnetic field, i.e., Larmor motion starts. This circular motion induces diamagnetic currents, sweeping aside the field of the chamber. The compressed field, however, pushes against the plasma, and finally redirects the plasma to produce thrust. The chamber has advantage in that its thermalization with the wall structures of the thrust chamber can be avoided.

Hyde [1] designed a LFR for the first time and estimated its thrust efficiency using a two-dimensional magnetohydrodynamics (MHD) code. The efficiency in terms of momentum was reported to be 65%, where the thrust efficiency is defined as the ratio of $\sum m_i v_z$ to $\sum m_i |v_0|$, where m_i is the ion mass, v_z is the z - component of its velocity and $|v_0|$ is the absolute initial velocity. The sum $\sum$ is carried over all the plasma particles.

Nagamine and Nakashima [2] have investigated (a) whether Rayleigh - Taylor instability is significant for the plasma expansion in the magnetic thrust chamber

and (b) how the efficiency for converting particle momentum into momentum along the rocket's thrust vector varies with certain parameters.

Zakharov et al. [3] reviewed the physical background of the magnetic thrust chamber and its laboratory verification in simulation experiments with laser - produced plasma cloud (LPC) expanding in an axially symmetric dipole magnetic field. As a result of such a kind of "Impulse" experiment under dimensionless conditions close to the related project of the interplanetary spacecraft $VISTA$ [4], [5], a conversion efficiency of plasma momentum as high as 60% was obtained in this type of magnetic thrust chamber for the first time by various independent methods.

Nakashima et al. [6] proposed to use ignition facilities such as National Ignition Facility (NIF) to examine the feasibility of the thrust chamber concept and to identify the plasma instability expected in the chamber since the facility could realize the same plasma conditions as supposed for the fusion rocket. However, before realizing such a real - scale demonstration, it is preferable to conduct a scaled - down experiment by which a direct comparison between numerical simulation and experimental efforts is possible. Such a comparison is important to understand the complicated physics of the magnetic thrust chamber. However, thus far, comparisons were made only for some early stages of the exploding plasma of the scaled - down model of the magnetic thrust chamber by Muranaka et al. [7]. They studied plasma behavior in a dipole magnetic field using a $3D$ hybrid code. Results for the early stages of plasma evolution of a scaled - down model of the magnetic thrust chamber are compared with the experimental and MHD analytical data of Nikitin et al. [8]. The dependence of plasma expansion on initial plasma energy and location are discussed by temporal evolutions of plasma position and magnetic field strength. Following the paper by Muranaka et al. [7], the present study attempts to obtain a complete plasma evolution of the scaled - down model numerically.

In this Chapter we discuss the experimental work for examining the thrust conversion process in the magnetic thrust chamber in the scaled - down model. The

expansion of LPC in the dipole field is studied under the conditions close to those in LFR magnetic thrust chamber [3]. In addition, we present the results of simulation studies using a $3D$ hybrid code to examine the plasma behavior in the chamber and to compare them with the experimental results for LPC.

The outline of this Chapter is as follows: In Section **3.2**, we discuss experimental parameters that are used in the LPC experiment [3] and the similarity criteria between the experiment and projects such as VISTA. The criteria are used to obtain the scaled - down model of the magnetic thrust chamber. Section **3.3** discusses the experimental setup. The analysis of plasma behavior in the magnetic thrust chamber, the estimation of thrust conversion efficiency and the comparison of the experimental results with the simulation ones are presented in Section **3.4** along with their discussion. The conclusions are given in Section **3.5**. Finally, in the Appendix, we specify how to obtain thrust efficiency by magnetic probe measurements.

3.2 Characteristics of plasma cloud expansion

Pioneer works related to the present topics were conducted by a Japanese group. Sato et al. [9] studied experimentally and numerically (1) the physical mechanisms by which the kinetic expansion energy of plasma is reconverted into thermal energy as the result of plasma - magnetic field interaction and (2) occurrence of plasma instabilities. Sudo et al. [10] discussed in detail the process of re-thermalization (reconversion from kinetic expansion energy of the ions to thermal energy of electrons through various physical processes). Okada et al. [11] have shown theoretically that lower - hybrid - drift instability could occur on the surface of the plasma column. When the radius of the column attains its maximum, the plasma luminosity (flute - like striation) is observed in Ref. [12]. Aizawa et al. [13] studied the plasma column behavior in presence of uniform axial magnetic field by using "two - and - a - half - dimensional" particle simulation code. It was found that the ion density contours exhibit a "crater - wall - like" structure and the profile of magnetic field value (B_z) exhibits a cavity ($B_z \simeq 0$) in the central part of the plasma cylinder.

Motivated by this, many works have been conducted, including the experiments [14] — [17], theoretical works and computer simulations [18] — [22].

The necessity to apply sophisticated PIC - models to describe the plasma cloud behavior in the magnetic thrust chamber is determined by the conditions of the collisionless expansion of ions with a small but finite directed Larmor radius R_L on the characteristic scale R_b of cloud deceleration by magnetic field $\vec{B}_{d0}$ of the coil, where

$$R_L = \frac{m_i \vec{V}_0}{Ze\vec{B}_{d0}}$$

and

$$R_b \approx \left(\frac{3\mu_0 E_0}{4\pi \vec{B}_{d0}^2} \right)^{1/3},$$

and m_i is the ion mass, $\vec{V}_0$ the initial velocity, Z the charge rate, e the elementary electric charge, μ_0 the vacuum magnetic permeability and E_0 the kinetic energy.

Retardation radius R_b is calculated under the condition that the kinetic energy density of all the plasma particles is equal to the density of the magnetic field energy. R_b accounts for the ideal characteristics of the retardation process, therefore some high - speed particles do not stop moving after R_b is reached.

As the result of Zakharov's experiment [17] on the interaction of LPC with a uniform magnetic field, the role of the general similarity criterion of problem $\varepsilon_b = R_L/R_b$ was established for exploding plasma clouds. The cloud interacts effectively with the field only under the condition of sufficient ion magnetization, i.e., $\varepsilon_b \leq 1$. In the opposite case, due to enhanced field penetration into plasma (with $\nu_{eff} \sim 0.3\,\omega_{ce}$ for electrons, where ν_{eff} is the electron turbulence frequency of the collisions and ω_{ce} is the electron cyclotron frequency), plasma cannot be decelerated by the field. One of the goals of the present "Impulse" experiment with LPC at the $KI-1$ facility was to check this critical ε_b for the case of a nonuniform dipolelike field typical of the LFR design [3] (see Table 3.1).

Table 3.1. Comparison of various parameters.

Parameter		$VISTA$ Project[4] for H_2-expellant	$VISTA$ testing at NIF[2],[6] (proposed)	$KI-1$[3], experiment
Kinetic energy	E_0	$500-1000\,MJ$	$4\,MJ$	$3-4\,J$
Exp. velocity	V_0	$300\,km/s$	$300\,km/s$	$140\,km/s$
Plasma ions	$\langle m/z\rangle$	$1\,amu\,(H)$	$\sim 10\,amu$	$2.6\,amu$
Ejection point	R_0	$11\,m$	$1\,m$	$15\,cm$
Magnetic field at R_0	B_{d0}	$4\,kG$	$9\,kG$	$1\,kG$
Coil current	J_c	$17\,MA$	$4\,MA$	$\sim 10^5\,(A-Turn)$
Coil radius	R_c	$13\,m$	$1\,m$	$\sim 5\,cm$
Magnetic moment	μ_d	$10^{13}\,G\cdot cm^3$	$10^{10}\,G\cdot cm^3$	$2\times 10^6\,G\cdot cm^3$
Ion magnetization	ε_b	~ 0.001	0.02	$\leq 1\,(<\varepsilon_{bc})$
criterion $\varepsilon_b = R_L/R_b$		$(\ll \varepsilon_{bc}\sim 1.3-1.5)$		
Energetic criterion	κ	$0.2-0.4$	~ 1	$0.1\,(<\kappa_c)$
$\kappa = 3E_0R_0^3/\mu_d^2$		$(\leq \kappa_c = 0.4)$		

Nikitin et al. [8] discussed the dynamics of the $3D$ expansion of a spherical cloud of rarefied plasma into a vacuum in the presence of a nonuniform external magnetic field of dipole structure, in the framework of ideal MHD approximation, and described how to determine the configuration and location of the plasma front as functions of time, and also how to determine the limits of its propagation, which are caused by the retardation effect. In addition, the authors of this paper defined another energetic criterion κ that characterizes the interaction between the expanding plasma and the dipole field and is given as

$$\kappa = \frac{E_0}{E_M} = \frac{12\pi E_0 R_0^3}{\mu_0 \left|\mu_d\right|^2},$$

where E_0 is the initial kinetic energy of ions, E_M the field energy integral of the dipole beyond the spherical radius R_0 $\left(E_M = (\mu_0/(4\pi))\left|\mu_d\right|^2 / \left(3R_0^3\right)\right)$, R_0 the distance from the magnetic coil to the explosion location and $|\mu_d|$ the magnetic moment magnitude. The critical criterion κ_c was found by Nikitin et al. [8] for a different plasma location. When κ is lower than κ_c, substantial plasma deceleration will occur in all directions from the explosion location ("quasi-capture" mode), while the plasma will not be captured by an ambient magnetic field when κ is greater than κ_c ("rupture" mode). (When the plasma is located at the axis, the critical value is $\kappa_c = 0.4$.)

Table 3.1 compares the main parameters of the scaled - down experiment considered here $(KI-1)$ and the parameters of projects such as $VISTA$. We can see that the criteria in the experiment satisfy the same conditions as those in the $VISTA$ project. The value of the energetic criterion of the problem $\kappa \sim 0.1-1$ was close to the range of the $VISTA$ project while the value of the general similarity criterion $\varepsilon_b = R_L/R_b \leq 1$ was sufficiently low to expect high diamagnetic properties of the plasma cloud.

3.3 Experimental setup

To simulate the real processes of plasma momentum transfer in a dipolelike magnetic field and to determine thrust efficiency, Zakharov et al. [3] have conducted the "Impulse" experiment as shown in Fig. 3.1 at the $KI-1$ facility [23] on the release of quasi - spherical LPC, with an initial expansion velocity V_0 of $\sim 140-200\,km/s$ and a total kinetic energy E_0 of $\sim 3-8\,J$ at the axis of the quasi - stationary ($\sim 1\,ms$) dipole with a moment $\mu_d = (1-2)\times 10^6\,G\cdot cm^3$, and a stainless-still spherical shell of radius $R_d = 8\,cm$. Plasma was generated at a background pressure of $\sim 0.001\,mTorr$ ($\sim 0.133mPa$) by means of CO_2 - laser beams with a total energy of $\sim 50-100\,J$ irradiating the Nylon 6 $(C_6H_{11}ON)_n$ pellet target of $3-4\,mm$ diameter (suspended by a thin metallic wire). The laser pulse of $70\,ns$ - duration was sufficiently short to fulfill the condition of instantaneous, explosion - like energy release of LFR - thrust and the thickness of the dipole shell (a few mm) was larger than the penetration depth of the magnetic field disturbances b_θ caused by plasma moment μ_c. Therefore the shell could imitate the presence of a metallic surface of the Li - shield and Al - constructions surrounding the superconducting coil of $VISTA$ [4].

For diagnostic purposes in the "Impulse" experiment (Fig. 3.1) we have used a set of double Langmuir probes, shielded B - dot magnetic probes and the same probes at the dipole shell to determine its impulse via b_θ - measurements. All systems of diagnostics had resolutions higher than $1\,cm$ and $30\,ns$, including a gated optical imager (GOI) that has registered the luminosity of the CIV - line (at $580\,nm$) excited by the charge - exchange of LPC ions in the presence of a specially added H_2 - gas with a pressure of $\sim (0.1-0.2)\,mTorr$. Such a method allow us not only to visualize but also to measure the spatial density distribution of the major C^{+4} - ion component of LPC (the other one is H^+).

3.4 Results and discussion

As mentioned in **Chapter 2**, $3D$ hybrid PIC code is used to calculate the plasma behavior under the dipole magnetic field. The code is based on the model given by Horowitz [24]. The hybrid code treats ions as individual particles and electrons as a fluid. This approach is valid when the system behavior is dominated by ion physics.

The equations controlling our system can be derived from Maxwell's equations and the equations of motion of particles.

In Ampere's law, Darwin approximation is made, that is, the transverse displacement current is neglected. We also assume quasi - neutrality and set the ion charge density equal to the electron charge density.

The calculation model considered here is illustrated in Fig. 3.2 and is based on the experiment performed by Zakharov et al. [3].

The general calculation parameters used in the simulation are shown in Table 3.2.

The initial distributions of the particle positions and velocities are assumed to be uniform. Here, the simulation starts from $t = 0.15\,\mu s$ to take into account of the time elapsed for the plasma expansion to $2\,cm$ in radius (we assume this, because until this time the plasma expands isotropically and there are no important changes in plasma shape). The initial plasma location is the same as in the experiment.

Here, we assume a single kind of plasma with a charge state Z of $+2.5$ and a mass of $6.5\,amu$ by taking the average quantities of two ions H^+ and C^{4+} produced in the experiment.

We will present the simulation results along with the experimental results.

Table 3.2. Calculation parameters.

Coil radius (m)	0.05
Coil current (A)	2.52×10^5
Coil position along Z (m)	-0.15
Plasma coordinates (m)	$(0, 0, 0)$
Plasma radius (m)	0.021
Plasma energy (J)	3.5
Plasma mass (g)	0.6×10^{-6}
Atomic mass (AMU)	6.5
Atomic number	2.5
Magnetic moment μ_d $(G \cdot cm^3)$	2×10^6
Initial magnetic field strength at the plasma (T)	0.1
Electron temperature (eV)	0
Initial max. velocity (km/s)	140
Time step Δt (μs)	0.000067
Calculation region (m)	$0.6 \times 0.6 \times 0.45$
Mesh size	$40 \times 40 \times 30$
Number of particles	100000

The numerical results for the time evolutions of particle position are shown in Figs. 3.3(a) and 3.3(b), where they are projected onto the XZ and XY planes, respectively. As is shown in these figures, the plasma shape is spherical at the initial stage and the plasma expands almost isotropically. Then the ions moving in the direction of the coil are reflected back by the magnetic field as explained in the **3.1** Introduction, and the shape of the plasma changes to follow the dipole magnetic field line. On the other hand, as shown in Fig. 3.3(b), the shape of the plasma is symmetric at all the stages in the XY plane.

Figures 3.4(a) and 3.4(b) show the time evolutions of velocity distributions projected onto the XZ and XY planes at early stages. The velocity vectors are directed and displaced according to the magnetic lines of force. In Fig. 3.4(b), we can see the ion Larmor rotation of the plasma particles related to the diamagnetic exclusion of the magnetic field in the plasma.

We could not observe any clear evidence of plasma capture, although the parameter κ ($\kappa = 0.1$) was much less than the critical value of 0.4. Note that this critical value is obtained using the idealized MHD - Nikitin model. (Strictly speaking, the present experiment and calculation are not of the MHD case, because for the MHD model to be valid, the similarity criterion $\varepsilon_b = R_L/R_b$ should be much less than the critical value of 1.0; in the present experiment $\varepsilon_b \sim 1$.) Many approximations are adopted in the derivation of the critical value, hence the MHD - Nikitin model fails to reproduce the experimental results.

The experimental results in Fig. 3.5 are obtained using GOI for the particle position projected onto the XZ plane at a time of $0.75\mu s$. The simulation result is shown as a dashed line in the figure. As seen from the picture, the plasma shapes are almost identical between the simulation and experiment, although the asymmetrical expansion in the experiment made closer comparison difficult. The asymmetrical shape of plasma expansion is related to the laser beam paths which corresponds to the preferable directions of plasma expansion (top right and bottom left). We proposed to use the *Gekko XII* facility in irradiating the target more uniformly [25], which will make possible a quantitative comparison. Note also that the jet towards the magnet collides with the shell in Fig. 3.5, while in Fig. 3.3 the jet runs through the magnet because the shell enclosing the magnet is neglected in the simulation (see Fig. 3.2).

Figure 3.6 shows the angular distribution of the plasma flow obtained by time integration of the data measured using double Langmuir probes in the experiment while Fig. 3.7 shows the distribution obtained by the simulation. Here, for com-

parison, we consider an arbitrary unit in Fig. 3.7, because we use discrete particles (each of which symbolized an action of many physical particles) in the simulation. For convenience, we used spatial integration instead of time integration, i.e., we registered the particles that locate beyond the radius of $25\,cm$ at $3\,\mu s$, since the particles will not significantly change the trajectories around this time. We can see from these figures that the plasma flow is collimated by a magnetic field within an angle of $\sim 60°$. On the other hand when a magnetic field is absent ($\vec{B}_{d0} = 0$), an isotropic plasma flow is obtained (see Fig. 3.6).

The experimental data on the magnetic field disturbances $\Delta\vec{B}$ caused by the diamagnetic cavity of plasma are illustrated in Figs. 3.8(a) and 3.8(b). The signals on these figures are simple trace of B - dot magnetic probes. The signals are registered using an oscilloscope. The total errors of measurements are approximately $(\pm)7\%$, relative to any current signal amplitude. Figures 3.9 and 3.10 show the simulation data of magnetic field disturbances $\Delta\vec{B}$, which are obtained at various points of the simulation.

Curve 2 in Fig. 3.9 is similar to curve 2 in Fig. 3.8(a), however the value of the field displacement for the simulation data is more than that of the experimental data. On the other hand, the time of the field displacement for the simulation data is shorter than that for the experimental data. The same situation is observed for both the curve in Fig. 3.10 and curve 2 in Fig. 3.8(b). The probable reasons for the differences is that the number of discrete particles used is not sufficient in the simulation (we use 100000 in this calculation). In particular, the probe location of curve 2 in Fig. 3.9 and Fig. 3.8(a) is along the Z axis ($\phi \approx 0°$), so the solid angle around the probe is very small and very few particles come to this region, which results in ambiguity in the simulation. Curve 1 in Fig. 3.8(b) and the curve 1 in Fig. 3.9 show a rather good agreement.

The thrust efficiency η in terms of the momentum is calculated as follows:

$$\eta = \frac{\sum m_i v_z}{\sum m_i |v_0|},$$

where m_i is the ion mass, v_z the z - component of its velocity and $|v_0|$ the absolute initial velocity. The sum is carried over all the plasma particles. The results are shown in Fig. 3.11 as functions of time. η increases rapidly between $0.1\,\mu s$ and $0.5\,\mu s$ and then its value saturates at approximately 60% at $3.0\,\mu s$ in Fig. 3.11. On the other hand, from the experimental result in Fig. 3.12, η reaches a value of about 60%, however it increases more gently as compared with the simulation result. The difference appeared because we assumed that at the initial stage of plasma expansion, particles and velocities distributions are uniform and the shape of the plasma cloud is spherical at this stage. The experimental value of η was obtained by measuring the impulse to the shell. The total measurement error of the thrust efficiency is approximately $(\pm)\,7\%$ of its maximum value (60%). The measurement accuracy of thrust efficiency (through the impulse of the shell derived using the probe at its surface) is defined by the accuracy of the measurement of the magnetic field disturbances b_θ caused by plasma moment, dipole field B_ρ and initial plasma impulse (measured using the Langmuir probes). So the curve of experimental efficiency results from the traces of B - dot magnetic probes at the dipole shell, integrated as $b_\theta B_\rho/\mu_0$ over its surface and current time [26]. (See the Appendix for more detailed explanation.) All signals are registered using an oscilloscope with subsequent digitalization. For the final value of η, a good agreement between the simulation and experimental results is obtained.

3.5 Conclusions

An experiment was conducted to study the thrust conversion process in magnetic thrust chamber for a scaled - down model. The temporal evolution of LPC expansion in a dipole magnetic field was examined and thrust conversion efficiency was estimated. For comparative purposes, we have carried out numerical analyses on plasma behaviors in the dipole magnetic field by using a $3D$ hybrid PIC code. An overall good agreement between the experimental data and the numerical analyses was found. It was then concluded that a thrust conversion efficiency as high as 60% is possible in the scaled - down model considered here. It was also found that the experiments will be very useful in developing magnetic thrust chamber designs and testing the basic features of the large - scale simulative thrust chamber experiments proposed for NIF. For future engineering applications, these results will be useful in designing an optimal configuration of the magnetic thrust chamber.

References

[1] HYDE R., WOOD L. AND NUCKOLLS J.: *AIAA Paper, New York N* 72-1063 (1972) 312.

[2] NAGAMINE Y. AND NAKASHIMA H.: *Fusion Technol.* **35** (1999) 62.

[3] ZAKHAROV YU.P., MELEKHOV A.V., POSUKH V.G. AND SHAIKHISLAMOV I.F.: *Current Trends in International Fusion Research* — Abstr. 4th Symp., (2001) 31.

[4] ORTH C.D., KLEIN G., SERCEL J., HOFFMAN N., MURRAY K., CHANG-DIAZ F.: AIAA-87-1904, (1987).

[5] ORTH C.D., KLEIN G., SERCEL J., HOFFMAN N., MURRAY K., CHANG-DIAZ F.: UCRL-96676, (1987).

[6] NAKASHIMA H., NAGAMINE Y., YOSHIMI N., ZAKHAROV YU.P. AND PONOMARENKO A.G.: *Fusion Eng. Design* **44** (1999) 359.

[7] MURANAKA T., UCHIMURA H., NAKASHIMA H., ZAKHAROV YU.P., NIKITIN S.A. AND PONOMARENKO A.G.: *Jpn. J. Appl. Phys.* **40** (2001) 824.

[8] NIKITIN S.A. AND PONOMARENKO A.G.: *J. Appl. Mech. Tech. Phys.* **34** (1993) 745.

[9] SATO K., OKADA S., KOGOSHI S., SUDO S., TSUJI H., OHWADANO Y., SEKIGUCHI T., KATSURAI M. AND TANAKA H.: *Plasma Phys. and Controlled Nuclear Fusion Research 1976,* **II** (1979) 567.

[10] SUDO S., SATO K., AND SEKIGUCHI T.: *J. Phys. D: Appl. Phys.,* **11** (1978) 389.

[11] OKADA S., SATO K. AND SEKIGUCHI T.: *J. Phys. Soc. Jpn.,* **46** No.1 (1979) 355.

[12] OKADA S., SATO K. AND SEKIGUCHI T.: *Jpn. J. Appl. Phys.*, **20** No.1 (1981) 157.

[13] AIZAWA M., OHSAWA Y., SATO K., KAMIMURA T., AND SEKIGUCHI T.: *Jpn. J. Appl. Phys.*, **19** No.11 (1980) 2211.

[14] DIMONTE G. AND WILEY L.G.: *Phys. Rev. Lett.*, **67** No.13 (1991) 1755.

[15] DICKINSON H., ET AL.: *Phys. Fluids*, **5** (1962) 1048.

[16] RIPIN B.H., ET AL.: *Phys. Rev. Lett.*, **59** (1987) 2299.

[17] ZAKHAROV YU.P., ORISHICH A.M., PONOMARENKO A.G. AND POSUKH V.G.: *Sov. J. Plasma Phys.* **12** (1986) 674.

[18] BRECHT S.H. AND THOMAS V.A.: *J. Geophys. Res.*, **92** (1987) 2289.

[19] SGRO A.G., ET AL.: *Phys. Fluids*, **B1** (1989) 1890.

[20] WINSKE D.: *Phys. Fluids*, **B1** (1989) 1900.

[21] HUBA J.D., ET AL.: *Phys. Rev. Lett.*, **59** (1987) 2971.

[22] HASSAM A.B. AND HUBA J.D.: *Phys. Fluids*, **31** (1988) 318.

[23] ZAKHAROV YU.P., ANTONOV V.M. AND MELEKHOV A.V.: *AIP Conf. Proc.* 369 (1996) 357.

[24] HOROWITZ J.E., SHUMAKER D.E. AND ANDERSON D.V.: *J. Comput. Phys.* **84** (1989) 279.

[25] NAKASHIMA H.: Presented at 4th US-Japan Workshop on Laser-Driven Inertial Fusion Energy Technology, Osaka University (2003).

[26] ZAKHAROV YU.P. AND NAKASHIMA H.: *Proc. 9 Int. Conf. Emerging Nuclear Energy Systems, Dan Knassim Ltd., Ramat Gan, Israel* **1** (2002) 319.

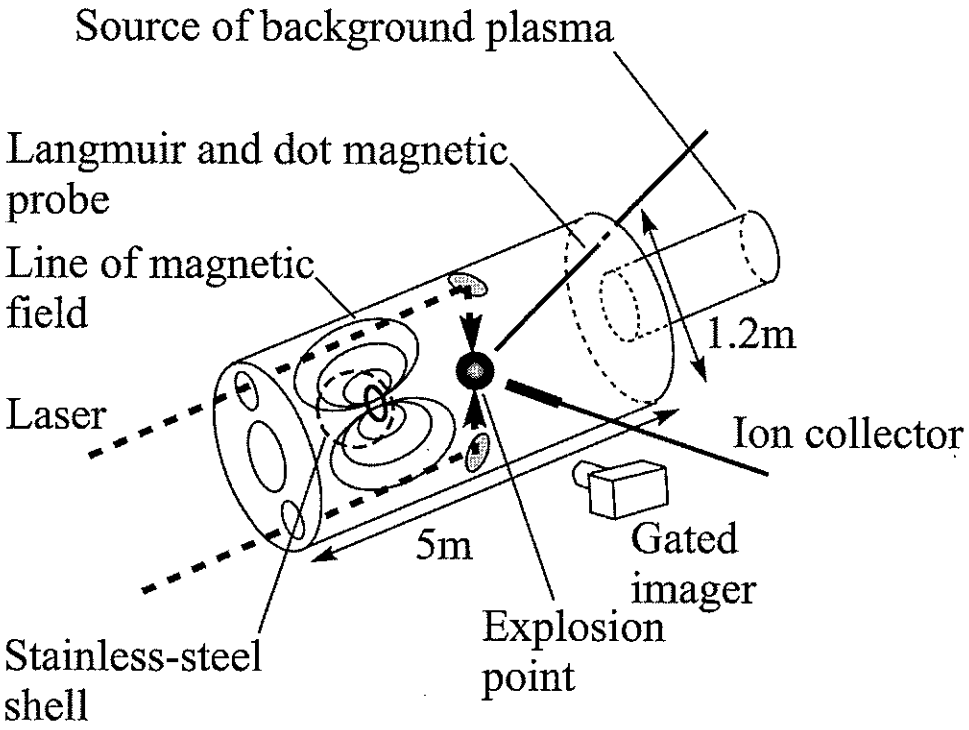

Fig. 3.1 Scheme of the experiment facility $KI-1$.

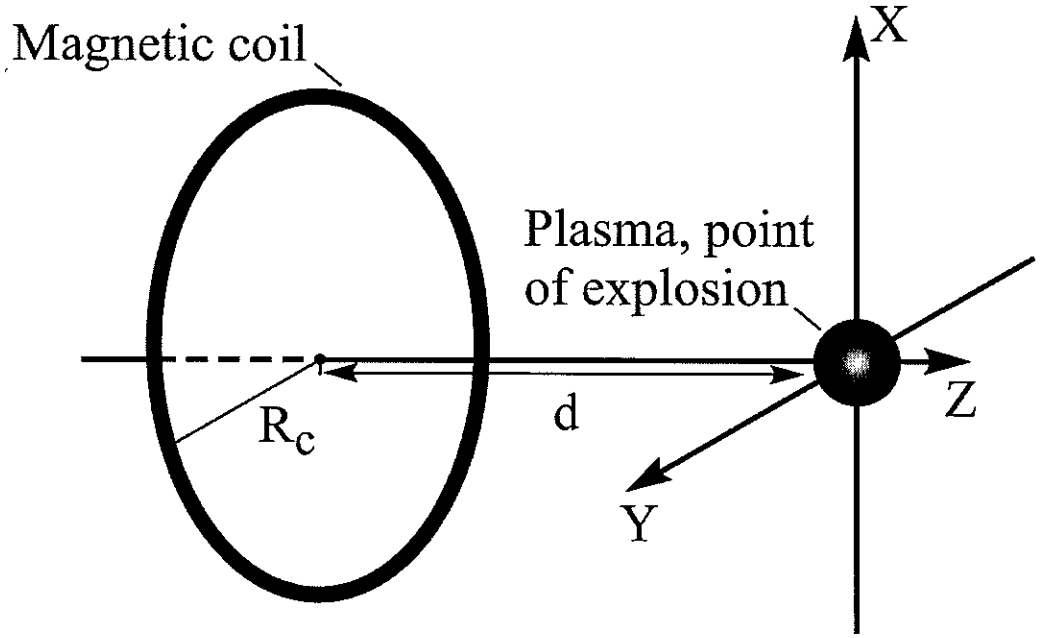

Fig. 3.2 Scheme of the calculation model.

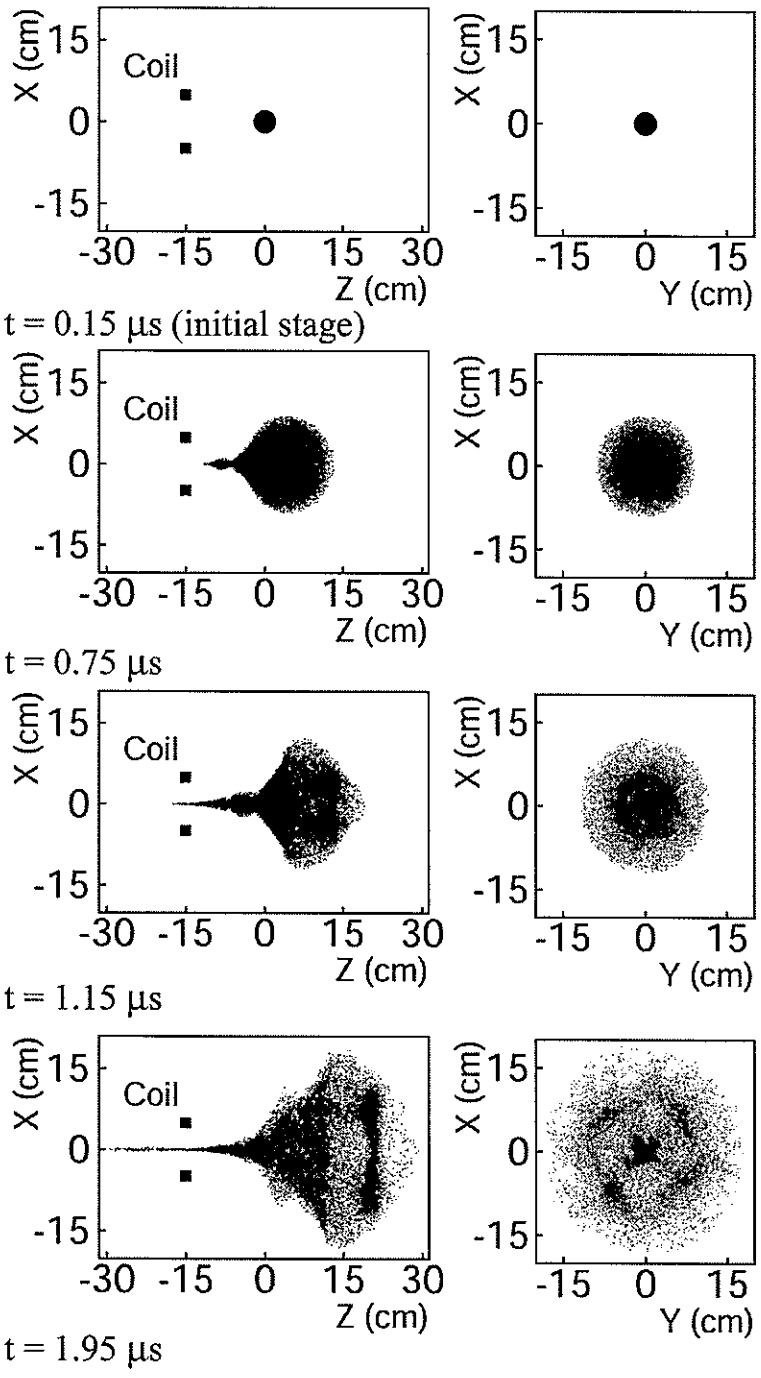

Fig. 3.3 Simulation results of particle positions projected onto the (a) XZ plane (left) and (b) XY plane (right).

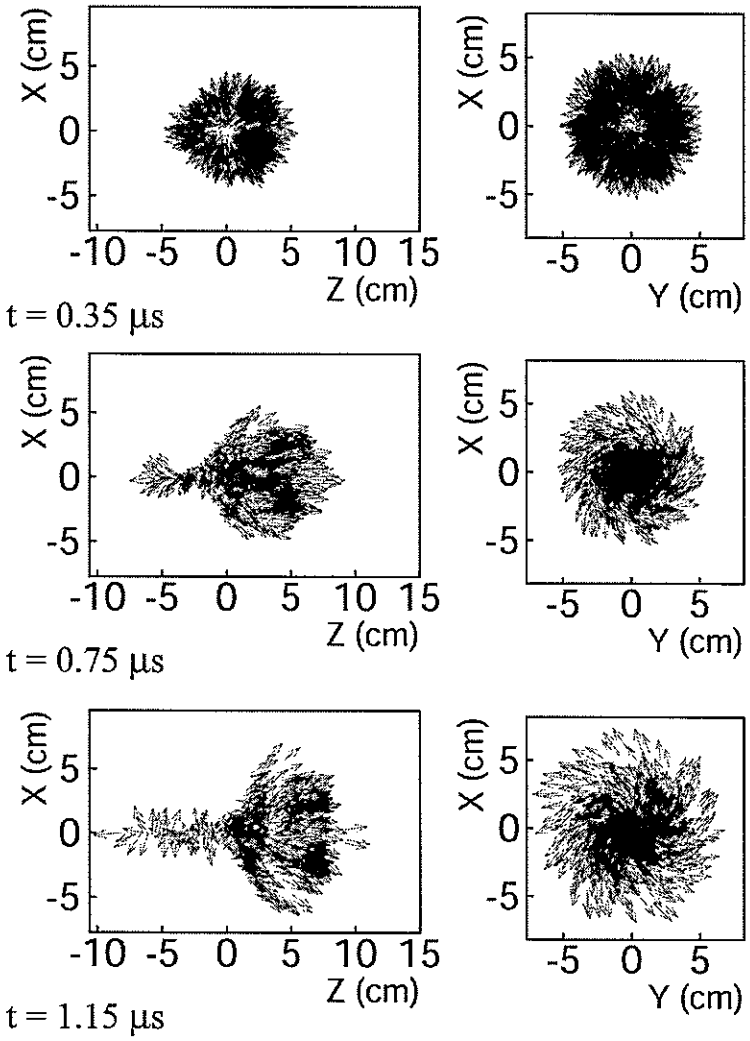

Fig. 3.4 Time evolution of velocity distributions at early stages projected onto the (a) XZ plane (left), and (b) XY plane at $Z \approx 5\,cm$ (right) (simulation results).

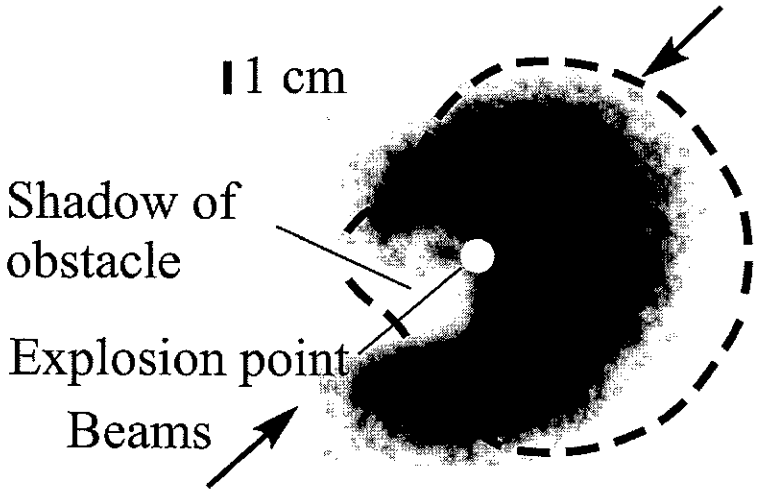

Fig. 3.5 Experimental results of the particle position projected onto the XZ plane at $0.75\,\mu s$. The dashed line is the particle position boundary of the simulation result.

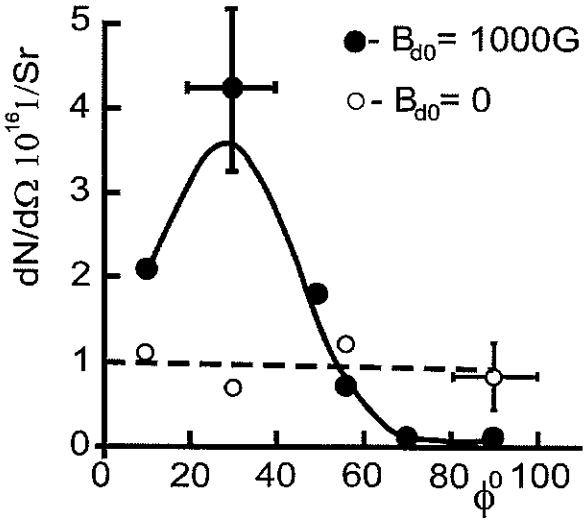

Fig. 3.6 Angular distribution of time-integrated plasma flow under conditions of LPC with $E_0 \sim 3 - 4\,J$ (experiment).

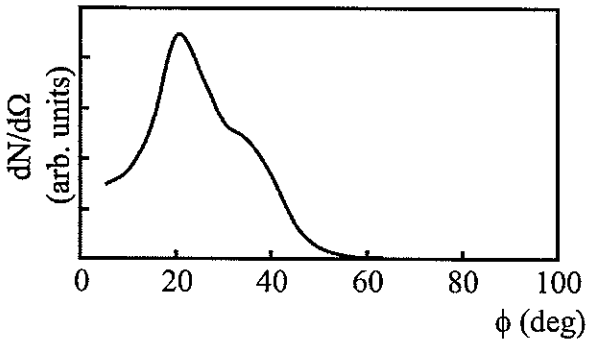

Fig. 3.7 Angular distribution of spatial - integrated plasma flow (simulation results).

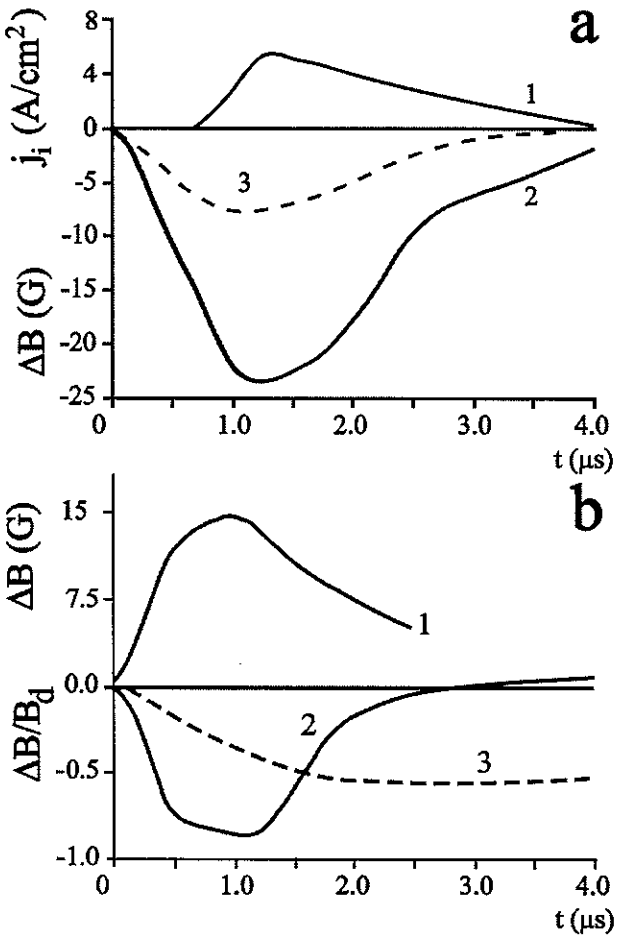

Fig. 3.8 The experimental data on magnetic field disturbances $\Delta\vec{B}$ caused by the diamagnetic cavity of plasma obtained at various positions of magnetic probes. (a) 1 plasma flow ($R_p \approx 25\,cm$, $\phi \approx 10°$), 2 $\Delta\vec{B}$ ($R_p \approx 16\,cm$, $\phi \approx 0°$), 3 $\Delta\vec{B}$ ($R_p \approx 21\,cm$, $\phi \approx 0°$); (b) 1 $\Delta\vec{B}$ ($R_p \approx 14\,cm$, $\phi \approx 90°$ – outside of LPC), 2 $\Delta\vec{B}$ ($R_p \approx 4.5\,cm$, $\phi \approx 45°$), 3 $\Delta\vec{B}$ ($R_p \approx 21\,cm$, $\phi \approx 0°$).

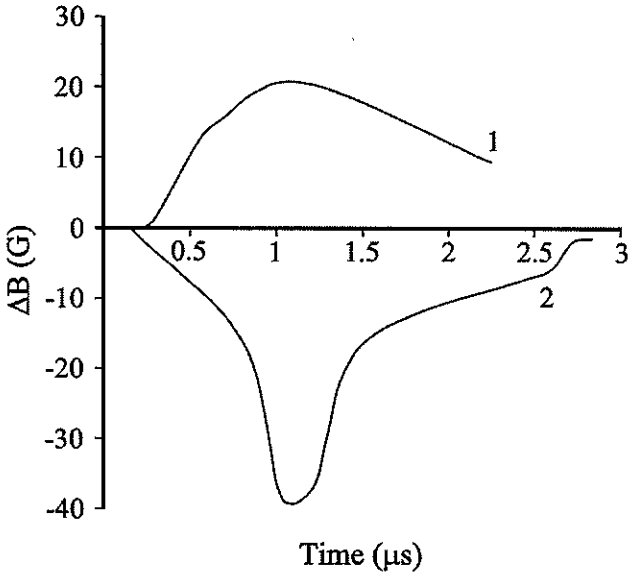

Fig. 3.9 Simulation data of magnetic field disturbances $\Delta\vec{B}$, 1 ($R_p \approx 14\,cm$, $\phi \approx 90°$, (cf. curve 1 in Fig. 3.8(b)), 2 ($R_p \approx 16\,cm$, $\phi \approx 0°$), (cf. curve 2 in Fig. 3.8(a)).

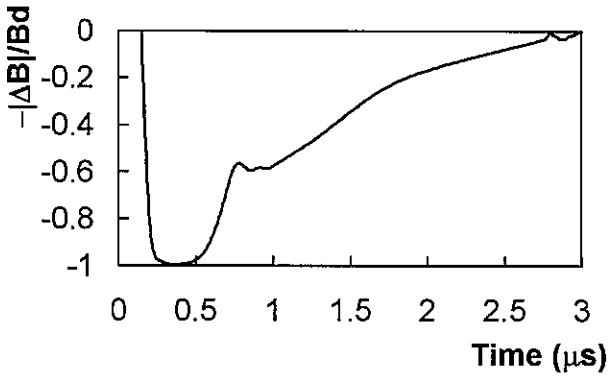

Fig. 3.10 Simulation data of magnetic field disturbances $\Delta\vec{B}$, normalized by the initial field $\vec{B}_d$ ($R_p \approx 4.5\,cm$, $\phi \approx 45°$), (cf. curve 2 in Fig. 3.8(b)).

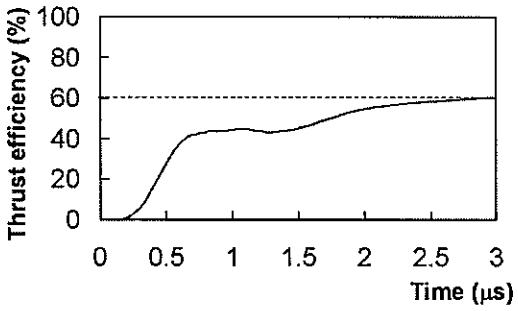

Fig. 3.11 Time evolution of thrust efficiency (simulation result).

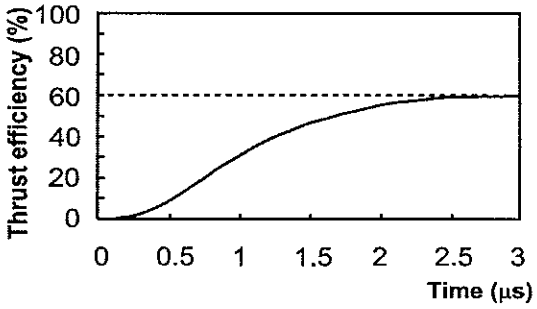

Fig. 3.12 Time evolution of thrust efficiency (experimental result).

4 Optimization of thrust efficiency in magnetic thrust chamber by using $3D$ hybrid PIC code

4.1 Introduction

In this Chapter we analyze the exploding plasma in a magnetic thrust chamber by using the three - dimensional hybrid PIC code and optimize the thrust efficiency by the same approach as in Ref. [1].

The approach is based on the analysis of retardation model of plasma cloud expansion under an ambient dipole magnetic field. The dimensions and configuration of the retardation region are estimated as functions of the initial expansion energy E_0. Configuration of magnetic walls (from which diamagnetic plasma radial flows are reflected) is found from the sectoral balance of the initial kinetic energy E_0 and work of ponderomotive forces and it depends upon the interaction parameter κ,

$$\kappa = \frac{3E_0R_0^3}{|\mu_d|^2},$$

where R_0 is the distance from the magnetic dipole to the explosion location and μ_d the magnetic moment. In particular, for the case of explosion at the polar axis the deceleration radius R_b making an angle θ with direction toward the dipole can be evaluated from the deceleration region equation as follows:

$$\kappa = 3\int_0^{R_b/R_0} \left\{3\left(1-x\cos\theta\right)^2/Q^4 + 1/Q^3\right\} x^2 dx, \qquad (4.1)$$
$$Q = Q(x,\theta) = 1 - 2x\cos\theta + x^2,$$

The deceleration regions found from equation (4.1) are shown in Fig. 4.1 for some values of κ in the YZ - plane [1].

As mentioned in Chapter 3 there is a critical value of the parameter $\kappa = \kappa_c$ ($\kappa_c = 0.1$ for the explosion at the magnetic equator, and $\kappa_c = 0.4$ at the axis [2]). When κ is lower than κ_c, substantial plasma deceleration will occur in all directions

from the explosion location ("quasi-capture" mode), while the plasma will not be captured by an ambient magnetic field when κ is greater than κ_c ("rupture" mode).

A scheme of magnetic nozzle in LFR with a deuterium - tritium pellet being located on the axis of a superconducting coil of radius R_c with the current J_c is to a certain extent in agreement with the case of the polar injection of the exploding plasma near the magnetic dipole. Evidently, the dipole approximation will be the most exact when $R_c \ll R_0$ [1].

It is convenient to analyze the thrust efficiency problem using an characteristic of the deceleration region such as a half angle of the plasma expansion cone α which in the dipole approximation is determined from the equation (4.1) when $R_b \to \infty$ (see Fig. 4.1).

The dependences of half angle of plasma expansion cone α on the energetic interaction parameter κ (the parameter characterizes the interaction between the expanding plasma and the dipole field, as explained in Chapter 3) and of the thrust efficiency η on the cone angle α are considered. In addition the authors of Ref. [1] compared their estimations with the results of numerical simulation by PIC code. According to the estimations the thrust efficiency amounts to about 85%.

The plan of this chapter is as follows: Section **4.2** presents the calculation model and method adopted here. The temporal evolution and integral - in - time picture of the exploding plasma in a dipole magnetic field, and estimation of the thrust conversion efficiency are presented in Section **4.3** along with discussion. The conclusions are given in Section **4.4**.

4.2 Numerical model

The calculation model considered here is illustrated in Fig. 4.2, and it is based on the simulation performed by Nagamine and Nakashima [3].

Cartesian coordinates are adopted here. The magnetic coil and the initial plasma cloud are located along Z - axis. The optimal distance between the plasma and the coil R_0 is defined according to the theoretical work of Nikitin and Ponomarenko [1] as:

$$R_0 = \left(\frac{\mu_d^2 \kappa_{opt} \mu_0}{12\pi E_0} \right)^{1/3},$$

where μ_d is the magnetic moment, E_0 the initial kinetic energy of ions and $\kappa_{opt} \simeq 0.5 - 0.6$.

Note an angle θ_C (cone angle) subtended from the initial plasma position at the Z - axis to the magnetic coil.

As mentioned above, the plasma behaviors are calculated by the $3D$ hybrid PIC code. The hybrid code treats ions as individual particles and electrons as a fluid. The equations controlling our system can be derived from Maxwell's equations and the equations of motion of the particles. The details are given in Chapter 2.

Calculations are performed for several cases with the different values of κ and ε_b, where ε_b is the general similarity criterion for the problem of the interaction of LPC with magnetic field (see Chapter 3). The common calculation parameters used in the simulation are shown in Table 4.1. The main parameters are the same as the simulation performed by Nagamine and Nakashima [3]. We have increased the interaction parameters κ and ε_b by changing the plasma cloud energy and the distance R_0 (see Table 4.2).

Initial distributions of the particle positions and velocities were assumed to be uniform. Here the simulation starts from $t = 0.8\,\mu s$ to take account of the time elapsed for the plasma expansion to $0.3\,m$ in the radius.

Table 4.1. Common calculation parameters.

Coil radius R_c (m)	1.0
Coil current (MA)	3.57
Coil position along Z (m)	-1.0
Plasma radius (m)	0.3
Plasma mass (g)	110×10^{-3}
Atomic mass (AMU)	197.0
Effective charge	16.81
Initial magnetic field strength at the plasma (T)	0.1
Time step Δt (μs)	0.00027
Calculation region (m)	$6 \times 6 \times 7$
Mesh size	$60 \times 60 \times 70$
Number of particles	100000

Table 4.2. Interaction parameters κ and ε_b for different cases.

Variants	#1	#2	#3	#4	#5	#6	#7[a]	#8[a]
κ	0.1	0.3	0.5	0.55	0.6	0.75	0.95	1.18
ε_b	0.02	0.02	0.03	0.03	0.03	0.03	0.03	0.03
R_0 (m)	1.0	1.0	0.80	0.83	0.85	1.0	1.0	1.0
Plasma energy (MJ)	0.42	1.25	4.0	4.0	4.0	3.14	3.9	4.9
θ_C (deg)	45	45	51.4	50.3	49.5	45	45	45

[a]From Ref. [3].

4.3 Results and discussion

In this section, we will present the simulation results along with discussion.

The numerical results for the time evolutions of particle position are shown in Figs. 4.3(a) and 4.3(b) for the case 5 (see Table 4.2), where they are projected onto the XZ and XY planes, respectively. As we can see in these figures, the plasma shape is spherical at the initial stage, and the plasma expands almost isotropically, and then the ions in the direction of the coil are reflected back by the magnetic field, and its shape changes to follow the dipole magnetic field line. On the other hand, as shown in Fig. 4.3(b) the shape of the plasma is symmetric at all the stages in the XY plane.

Figure 4.4 shows a time - integrated picture of plasma cloud, which was obtained by simulation. The simulation results were obtained by superimposition of plasma particle positions. The picture of the exploding plasma shows a cone - like geometry. The half angle of the plasma expansion cone α is estimated to be about 50°.

Note that there may be some ambiguity in determining the expansion angle α because in our case we are estimating the angle by the time - integrated picture of plasma cloud (see Fig. 4.4). Nikitin et al. [1] estimated the plasma expansion cone from the "deceleration region" equation (4.1).

Figure 4.5 shows the dependence of η on the expansion angle α, where the simulation results are shown as the points, and the solid line is obtained from the theoretical work of Nikitin et al. [1]. A too narrow cone ($\alpha \to 0$) as well as a too wide one ($\alpha \to \pi/2$) corresponds to the decrease in the thrust efficiency [1]. The maximum value of η reaches about 85% at $\alpha = \alpha_{opt} \simeq 45 - 50°$ in the MHD theoretical work. However, from the simulation result we can see that its maximum value of η reaches about 70% with $\alpha = \alpha_{opt} \simeq 45°$.

The dependence η on κ is shown in Fig. 4.6. In this figure, the theoretical result (solid line) is given for the value of κ which is larger than κ_c, although the simulation result is considered with κ less than κ_c. In our simulation, we could not

observe any clear evidence of the plasma capture, such as a substantial deceleration of plasma in all directions from the explosion location at the initial stage of the expansion, although the parameter κ was much smaller than the critical value $\kappa_c = 0.4$. However, in the MHD model, the plasma will be captured for the parameter range, and then the efficiency is zero as shown by the solid line.

The maximum value of η reaches about 85% at $\kappa = \kappa_{opt} \simeq 0.5 - 0.6$ in the MHD theoretical work. However, from the simulation result we can see that the maximum value of η reaches about 70% with $\kappa = \kappa_{opt} \simeq 0.5 - 0.6$. Points 3, 4 and 5 have the same values of η because the cone angle θ_C is about 50° for these points [3] (see Table 4.2). Points 7 and 8 were obtained from Ref. [3] and displayed here for comparison.

The MHD theoretical work of Nikitin S. [1], [4] is so ideal, because many assumptions were made for the theoretical equations. In the theoretical model the basic principles of the three dimensional dynamics of the plasma cloud retardation are based on some simple relations for generalized characteristics of motion: energy and pressure. The role of magnetic diffusion is not taken into account. These assumptions partly explain the differences between theoretic and simulation value of η.

4.4 Conclusions

Optimization study on the thrust efficiency was performed for the magnetic thrust chamber by the $3D$ hybrid code. Initial plasma cloud is located some distance along the magnetic coil symmetric axis. Calculations are performed for several cases with different values of energetic parameter κ (the parameter characterizes the interaction between the expanding plasma and the dipole field). Temporal evolution of plasma cloud expanding in a dipole magnetic field was examined. The time - integrated picture of plasma cloud shows a cone - like geometry and the half angle of the plasma expansion cone α was estimated.

Overall qualitative agreement between the simulation and the theoretical model of Nikitin and Ponomarenko [1] was found for the dependences of η on α and κ. However, the quantitative agreement was not obtained for the value η; in the theoretical model η amounts to 85%, while in the simulation the maximum η is 70%.

References

[1] NIKITIN S.A. AND PONOMARENKO A.G.: *Proceedings of the* 9^{th}, *ICENES*, Tel - Aviv, Israel (1998) 299.

[2] NIKITIN S.A. AND PONOMARENKO A.G.: *J. of Applied Mechanics and Tech. Phys.*, **36** No.4 (1995) 483.

[3] NAGAMINE Y. AND NAKASHIMA H.: *Fusion Technol.*, **35** (1999) 62.

[4] NIKITIN S.A. AND PONOMARENKO A.G.: *J. of Applied Mechanics and Tech. Phys.*, **6** (1993) 3.

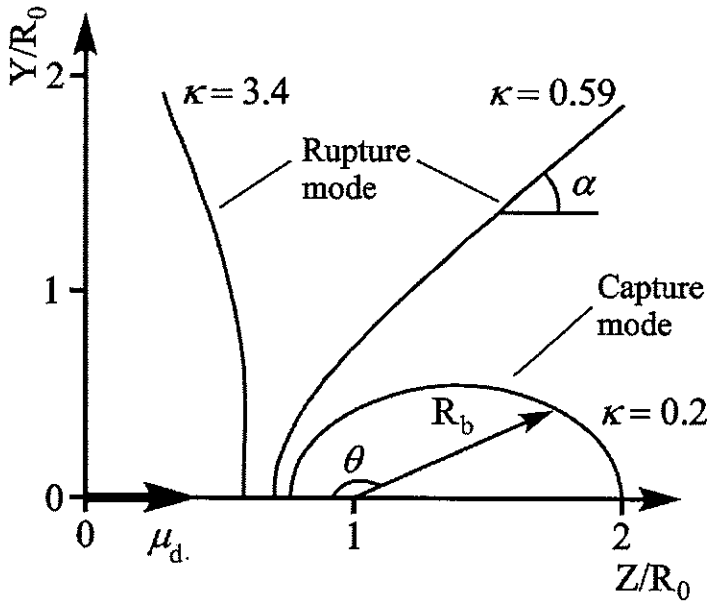

Fig. 4.1 Deceleration region meridional sections obtained from the theoretical deceleration region equation (Nikitin et al. [1]).

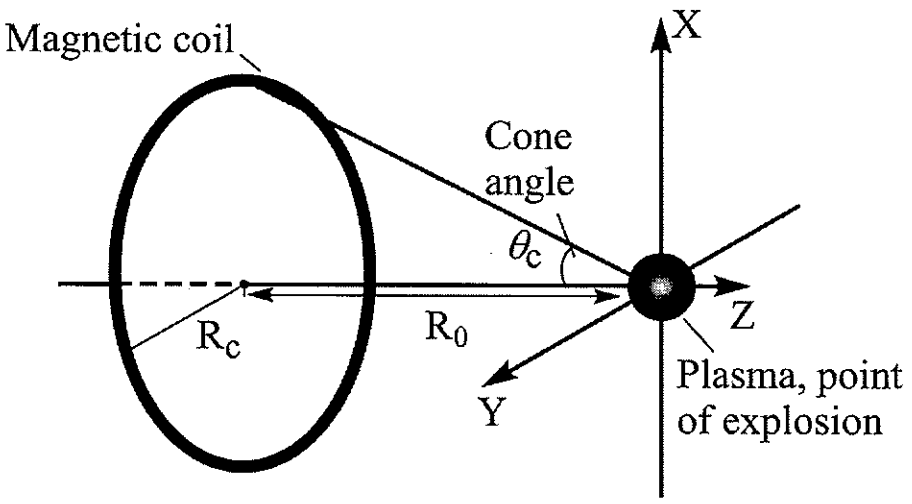

Fig. 4.2 Schematic of the calculation model.

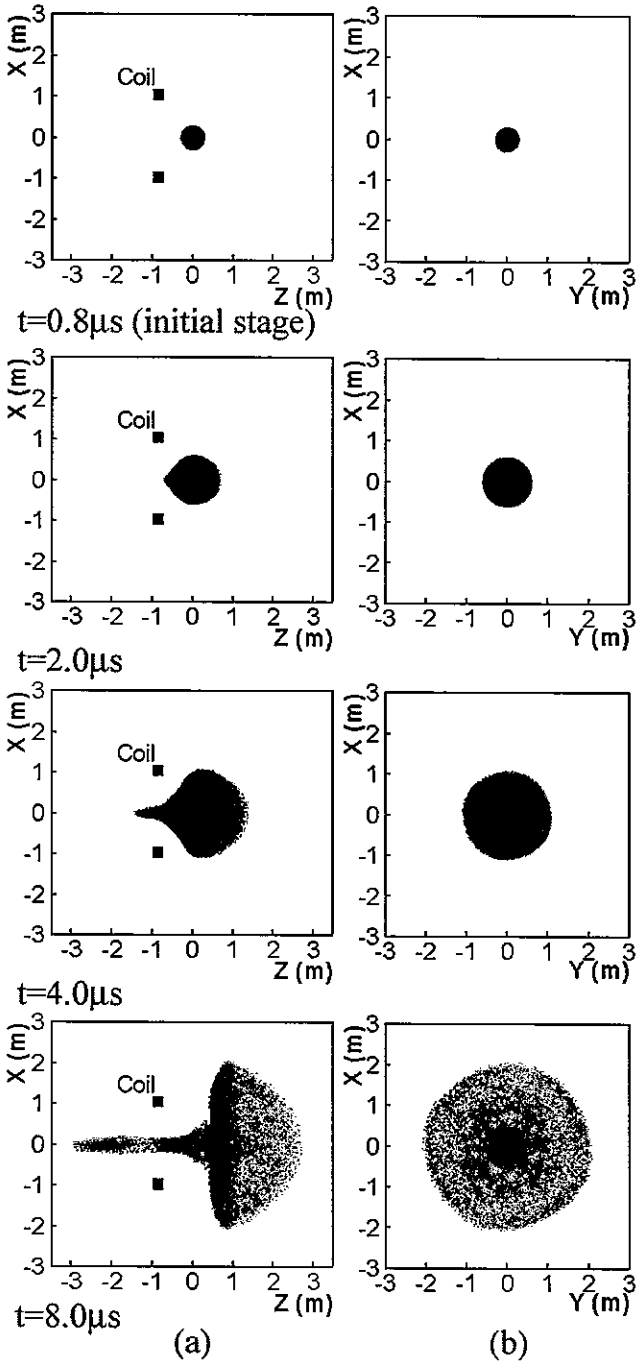

Fig. 4.3 Simulation results of particle positions projected onto the (a) XZ plane and (b) XY plane (Case 5: $R_0 = 0.85\ m,\ \kappa = 0.6$).

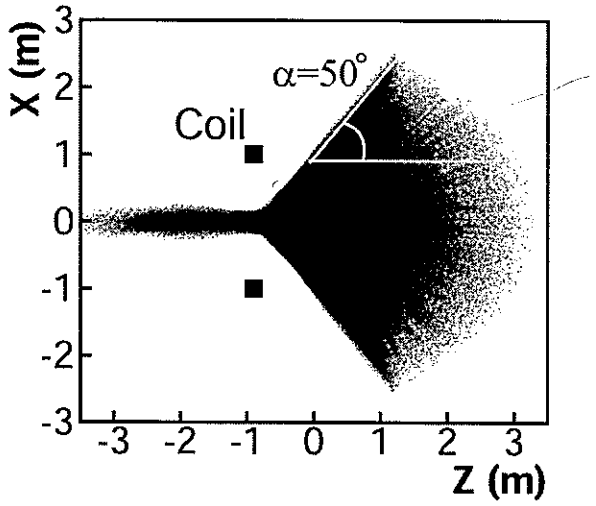

Fig. 4.4 Time - integrated picture of plasma cloud (simulation result, Case 5: $R_0 = 0.85m$, $\kappa = 0.6$).

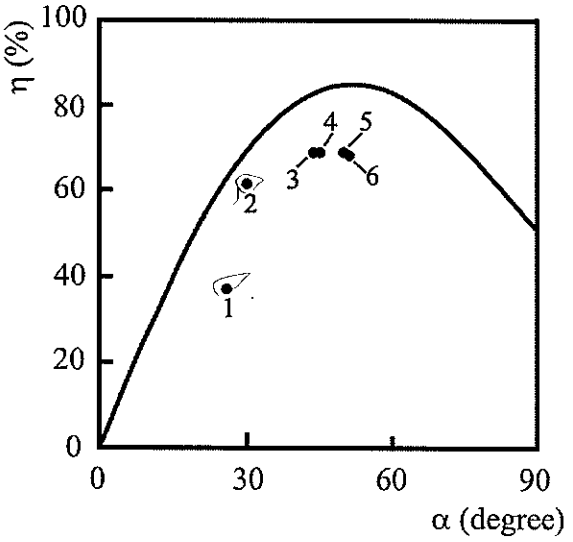

Fig. 4.5 Dependence η on α; 1 $\kappa = 0.1$, 2 $\kappa = 0.3$, 3 $\kappa = 0.5$, 4 $\kappa = 0.55$, 5 $\kappa = 0.6$, 6 $\kappa = 0.75$. Solid line is the theoretical result (Nikitin et al. [1]).

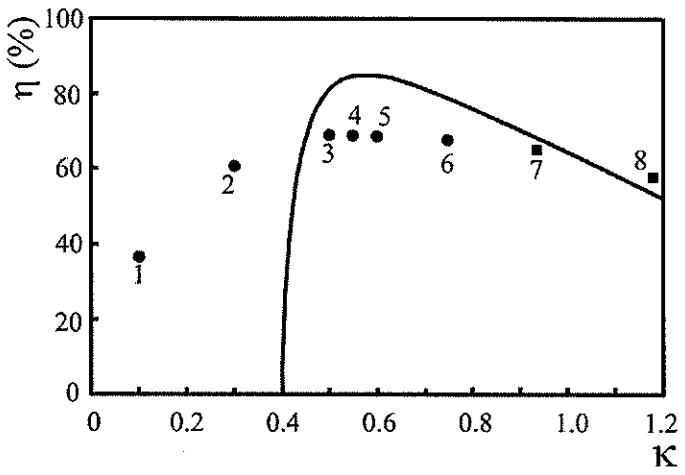

Fig. 4.6 Dependence η on κ; 1 $\kappa = 0.1$, 2 $\kappa = 0.3$, 3 $\kappa = 0.5$, 4 $\kappa = 0.55$, 5 $\kappa = 0.6$, 6 $\kappa = 0.75$; 7 $\kappa = 0.95$; 8 $\kappa = 1.18$. Solid line is the theoretical result (Nikitin et al. [1]). Points 7 and 8 from Nagamine and Nakashima [3].

5 Direct conversion of the plasma clouds energy into electrical energy during the expansion in a magnetic field

5.1 Introduction

Progress in designing Megajoule lasers such as National Ignition Facility (NIF) in $U.S.A.$, Laser Megajoule project (LMJ) in France and $KONGOH$ in Japan for inertial confinement fusion (ICF) has recently revived the interests in pulsed methods of direct conversion of fusion energy in magnetic field system [1] — [3].

In inertial confinement rocket some part of initial plasma energy could be directly transferred into electric energy by magnetic field for supplying the power of driver. The rest of the plasma energy is used to produce thrust. The power flow diagram is shown in Fig. 5.1. Fusion pellets are injected into a magnetic thrust chamber. At the same moment, the driver is fired to induce the micro - explosion in the pellets. The resulting fusion output is converted into thrust. Some of the fusion energy is picked up to power - supply the driver for next shot.

The method considered here is based on the general idea proposed by Artsimovich [1] and applied by Haught et al. [2]. This idea is to use coils that enclose an expanding diamagnetic plasma cloud. When the external magnetic field is excluded by the plasma and an inductive electromotive force ($e.m.f.$) is thus induced, currents J should be generated in the coils in the presence of load.

The scheme of energy recovery circuit that uses a capacitor with a diode is shown in Fig. 5.2. The breaker is conducting in the plasma expansion phase. At the moment when the plasma reaches its maximum radius and the coil induced current reaches its maximum value, the breaker is opened. The electric energy in the coil is dumped into the capacitor through the diode.

Levin [4] considers the problem of the interaction of a current ring with a perfectly conducting sphere with the center on the axis of the ring and shows that the exact solution of the problem can be obtained by using the method of images.

The method of images means as follows. For convenience the author changes the system of the currents on the surface of perfectly conductive sphere into the current of the coil image. Hence, in the case, the field outside the sphere is the sum of the fields generated by the current in the ring and by the current of its image. It allows to obtain the difference of the real coil inductance L and calculate the interaction force between sphere and coil.

The paper of Beloozerov [5] is dedicated to the interaction process of the perfectly conducting sphere (plasma cloud) with the magnetic field of a system of current coils. The author considers the axial and transverse stability of the equlibrium of a small perfectly conducting sphere in a system of coaxial ring currents.

Mima et al. [6] described a direct energy conversion method for $D-^3He$ inertial confinement fusion reactor. The method utilizes inductive energy recovery through pickup coils in the plasma chamber in which the mirror magnetic field is applied.

In the paper the authors propose schemes and configuration for the ICF reactor. The discussed schemes allow:

— To protect the chamber wall from sputtering and to remove intense radiation and neutron energy.

— To reduce the need to handle high voltage along the pickup coil. The one - turn pickup coil is divided into a number of pickup segments both axially and azimuthally so that it can be managed by near - term technologies.

— To continue inductive energy recovery after radial expansion.

Analytical results of the paper predict that the expanding plasma energy is directly converted to electricity through the recovery circuit using capacitor with an efficiency of more than 80% when the plasma is assumed to expand cylindrically.

Nakashima et al. [7] performed two - dimensional $R-Z$ geometry particle simulation of the plasma behavior in the $D-^3He$ reactor considered in Ref. [6].

The calculation model considered is based on the work by Dickman et al. [8]. According to the work the electromagnetic fields are assumed to be completely

described by the θ (azimutal) component of the magnetic vector potential A_θ, which means that the magnetic field components B_r and B_z and the inductive electric field E_θ are computed, but B_θ and all electrostatic fields are assumed to be zero.

In addition the authors give a brief explanation of the simulation code. A set of calculations was made for different values of the magnetic field intensity.

The results of the simulation analysis indicate that the energy extracted from the pickup coil system is $\sim$ 20% of the plasma energy during the first bounce motion of the plasma in the magnetic field of the reactor.

The detailed study fully taking into account of the actual geometry of the ICF reactor is performed by Shoyama et al. [9]. The authors studied the direct energy recovery from the pickup coil system by using a capacitor diode load circuit as an alternative to the resistive load one. For comparative purposes, the scheme of resistive circuit considered in Ref. [7] is also given.

Two calculation models were considered. First of all, one - dimensional calculation model is considered and the authors show that the direct energy recovery efficiency of 100% can be expected in the case. In the second phase, a two - dimensional $R - Z$ geometry calculation model was discussed.

The plasma behavior in the reactor is analyzed to estimate the efficiency of the direct energy recovery system. The results of the two - dimensional particle simulation indicate that the energy extracted from the direct energy recovery system using the capacitor diode load circuit is 70 $\sim$ 80% of the plasma energy at the maximum plasma expansion in the applied magnetic field of the reactor.

Zakharov et al. [10] have dealt with a promising method of direct energy conversion. The method described in detail allows to perform direct conversion of the kinetic energy of expanding plasma cloud into electrical energy. The conversion is realized due to inductive generation of currents in short - circuited load coils that enclose the plasma and are oriented across the external magnetic field. The authors discuss the physical and electrotechnical principles of the method.

An analysis of plasma deceleration by a magnetic field and transfer of plasma energy into an inductive load gave a solution of the problem in general form and the dimensionless parameters of the problem. The parameters determine the deceleration radius, the coil current and the theoretical conversion efficiency.

"Generator" experiment with the laser - produced plasma clouds on $KI-1$ facility to study conversion efficiency was performed. A comparison analysis of the experiment results and available numerical ones shows that the conversion efficiency as high as 30% can be achieved in the optimized version of the method for conversion of ICF energy.

To illustrate a real feasibility and possible very high effectiveness (more than 50%) of the direct energy conversion Zakharov et al. [11] discuss in detail basic physical processes and the methods of circuit loading of electrical energy generation systems with pickup coils in uniform initial magnetic field.

The values of generated coil current were estimated due to different approximations as follows. In the context of simplest (zero) approximation the back action of the pickup coil current field on the plasma deceleration is neglected. Other approximation takes into account the mutual inductance of plasma and pickup coil.

The predicting equation of optimal conversion regime was obtained. The authors show that the data of relevant $PIC-$ simulation do not contradict with the equation. According to the predicting equation the maximal conversion efficiency value of 32% could be achieved with its possible increasing up to 40 - 45%.

For the $VISTA$ design, about 5% is assumed for the conversion efficiency by using one pickup coil.

Various authors [12] — [17] have stated that it may be possible to directly convert some of the energy to electricity by allowing the plasma to expand and work against the magnetic field.

In this chapter, for comparative purposes, numerical analysis on the energy conversion are being conducted using the $3D$ hybrid PIC code. In this study for

investigating the conversion process of initial kinetic energy E_0 of plasma cloud into electrical energy E_e we are comparing the efficiency η of such conversion process between experiment and simulation. The conversion efficiency η is defined here as $\eta = W_{max}/E_0$, where W_{max} is the highest inductive energy obtained for one coil.

In Section **5.2** the simulative experiment "Generator" is discussed. The experiment was performed by Zakharov et al. [10] at $KI-1$ facility. For the problem of direct energy conversion, a calculation model, brief explanation of a part of simulation code which corresponds to the problem and description of the modification of the basic equations are presented in Section **5.3**. The calculation results are presented in Section **5.4** along with discussion. Finally, Section **5.5** is devoted to the summary and conclusions.

5.2 Simulation of ICF energy conversion in "Generator" experiment

Investigation of the inductive method of ICF energy conversion requires both a general analysis of the physical process of conversions of plasma energy and model experiment. The experiment is especially important because many of the indicated processes cannot be described by ordinary MHD equation (or adequately reproduced in purely collision - free calculations by the PIC method) provided that the ion Larmor radius is finite ($R_L \leq R_b$). This relation for values of the "directed" ion Larmor radius is typical of the parameters for the designed ICF reactors with a magnetic field [9] and can lead to anomalously fast development of flute instability at the cloud boundary [10], enhanced penetration of the field into the cloud with turbulent collision frequency $\nu_{ef} \approx 0.3\omega_{ce}$ (where ω_{ce} is the electron cyclotron frequency) of electrons [17], and electron heating [18]. The influence of these and other effects on the direct inductive conversion of the cloud energy and the real conversion efficiency were examined in the "Generator" experiment.

To simulate the real processes of direct conversion of the plasma clouds energy E_0 into the electrical energy E_e and to determine the conversion efficiency η, Zakharov et al. [10] have conducted the "Generator" experiment as shown in Fig. 5.3 at $KI-1$ facility [19].

In the "Generator" experiment (see Fig. 5.3), a caprolon ($C_6H_{11}ON$) spherical laser target of diameter $D \approx 3-4\ mm$ was irradiated on two sides in a direction transverse to the field by identical laser beams with cross - sectional diameter of about $2D$ (in the region of the target) and with total energy of $Q_0 \approx 100\ J$ in a CO_2 laser pulse with a duration of 100 $nsec$ and a wavelength of 10.6 μm. In the basic mode of experiment (field $B_0 = 500-620\ Gs$), the initial parameters of a quasistatic LPC with a total energy of $E_0 \approx 8J$ are characterized by a velocity of $V_{0\|} \approx 200km/sec$ along the beams and a velocity of $V_{0\perp} \approx 170km/sec$ across them.

The characteristic value of $\varepsilon_b \approx 0.7$ was small enough, but with decrease in the laser energy to $Q_0/3$ it could exceed the critical value of ε_b^*. As shown in the ex-

periment and grounded theoretically, for number of particles $N_i \gg 1$, dimensionless initial velocity of the plasma $V_0/c \ll 1$ and the relation $Zm_e/m_i \ll 1$ (where Z is the effective charge, m_e the electron mass and m_i the ion mass) the parameter $\varepsilon_b = R_L/R_b$ is the main similarity parameter of the problem with the critical value of $\varepsilon_b^* \approx 1.3 - 1.7$, where R_L is the directed Larmor radius of the ions and R_b is the retardation radius of the plasma cloud. Only for values $\varepsilon_b \leq \varepsilon_b^*$ the plasma cloud can be decelerated by the magnetic field to the velocity $V \approx V_0/2$ at the radius R_b and produce the diamagnetic cavity of the same size necessary for effective transfer of the plasma energy to the load in the presence of coil [10], [11].

Under the conditions, current generation in three types of short - circuited coils with dimensions close to R_b and basically elliptic configurations were explored. In the configurations the asymmetry of plasma expansion was accounted for by orientation of the minor semiaxis of the coil R_c^{min} along the radius R_b^{min}. The effects of plasma deceleration and formation of cavity were studied in the experiment.

In the experiment the coil current J was measured by a shielded Rogowski loop. The initial parameters and deceleration of the LPC outside the radius and plane of the coils were measured by Langmuir double probes. The dynamics of the plasma and the cavity inside the coil were examined using a gated optical imager (GOI) and miniature shielded magnetic probes. All indicated system of plasma diagnostics had an enough resolution ($20 - 30$ $nsec$) and plasma expansion transverse of the field was recorded by the GOI.

The main results of basic mode of the "Generator" experiment such as dynamics of the coil current, field exclusion inside the coil and dynamics of plasma expansion are compared with simulation ones in Section **5.4** along with discussion.

5.3 Calculation model and methods

In this section we will discuss about the calculation model and the numerical methods adopted here for the problem of direct energy conversion.

The calculation model considered here is illustrated in Fig. 5.4 and is based on the experiment performed by Zakharov et al. [10].

For analysis of plasma energy conversion to electrical energy, we consider an ideal system consisting of an initial spherical plasma cloud of radius R_p. The plasma is simulated by the set of the discrete particles (the model particle symbolizes an action of many physics particles) and is located in the center of the pickup coil of radius R_c. The plasma cloud and the pickup coil are located in an external magnetic field B_0 perpendicular to the plane of the coil.

The initial distribution of the particle positions and velocities are assumed to be uniform.

The calculation flow for the pickup coil system is shown in Fig. 5.5.

The subroutines of the part 1 "Initial preparation of 3D hybrid code" shown in Fig. 5.5 perform the following functions:

— read the initial data;

— normalize variables;

— set the initial values of the external magnetic field components;

— calculate the initial values of particle velocities;

— calculate the initial values of current density components;

— calculate the initial particles distribution.

The subroutines of the part 3 "Subroutines of 3D hybrid code" shown in Fig. 5.5 perform the following functions:

— calculate the components of the electric and magnetic fields;

— perform the calculation of particles motion, i.e perform the calculations of particle velocities and coordinates.

The subroutine of the last part 4 "Save data" in Fig. 5.5 performs the following function:

— save the calculation data for future treatment or continuation of the calculation.

Parts 1, 3 and 4 (see Fig.5.5) correspond to the parts of 3D hybrid code. The parts were described above (Chapter 2), and they are briefly considered here in a context of pickup coil subroutine.

In this section, the parts which correspond to the pickup coil system are described.

The pickup coil subroutine is shown in the box 2 of Fig. 5.5. The subroutine is located at the iteration cycle of time in the main code. The main purposes of the subroutine are calculations of the pickup coil current and the coil magnetic field for taking into account the influence of the coil magnetic field onto plasma retardation.

The part 2.1 in Fig. 5.5 "Calculation of the cavity maximum radius" calculates the cavity radius R_{cav}. Let us assume that at nodes with numbers $(i-1)$ and i, the values of magnetic field are B_1 and B_2 respectively, α is the angle of triangle DAE and B_0 is the value of initial magnetic field as shown in Fig. 5.6. From the triangle DAE, $\tan\alpha$ is $(B_2 - B_1)/DX$, where DX is the mesh size. On the other hand from the triangle CAF, $\tan\alpha$ is $(B_0 - B_1)/dr$, where dr is the distance between the value of x that corresponds to the initial magnetic field B_0 and the nearest node $(i-1)$ of the mesh on the left side. In that way we have

$$\tan\alpha = \frac{B_0 - B_1}{dr} = \frac{B_2 - B_1}{DX}, \quad \text{and} \quad dr = \frac{B_0 - B_1}{B_2 - B_1} DX.$$

Finally R_{cav} is calculated as follows.

$$R_{cav} = DX\,(i-1) + \frac{B_0 - B_1}{B_2 - B_1} DX. \tag{5.1}$$

In the last equation (5.1) we suppose that the cavity center is located in the center of coordinates, because in our case the plasma cloud center is located in the same point.

So, the algorithm of the cavity calculation is as follows.

Step 1. While $B_i \leq B_0$, the number of mesh node is increased as $i = i + 1$ (B_i is the magnetic field which corresponds to the mesh node with number i).

Step 2. When $B_i > B_0$, we suppose that the cavity is reached and the cavity radius is calculated from equation (5.1).

The cavity radius is an important parameter for such an energy conversion process, because the maximum cavity radius reaches when the coil current reaches the maximum value.

In the part 2.2 of Fig. 5.5 "Calculation of the pickup coil current" the pickup coil current is calculated as follows.

For calculating the maximum current of the pickup coil, the coil real inductance and useful energy we take up the same approach as in Ref. [10].

The coil inductance L is evaluated by taking into account the effect of the mutual inductance of plasma sphere and pickup coil. Due to presence of spherical cloud inside the coil, the coil inductance is approximated by

$$L \approx L_0 \left(1 - KX^3\right), \tag{5.2}$$

where L_0 is the coil self-inductance and $X = R_{cav}/R_c$, where R_c is the coil radius. The coil inductance could be characterized by an additional parameter $K \approx 3.6/\ln G$ on the base of "image" method [4], where $G = R_c/r_c$ for the radius r_c of the coil wire.

By using the conservation condition of the total flux inside the coil and analyzing the balance of the flux variations we can also determine the generated pickup coil current. According to the "image" method [4], the system "coil - plasma sphere" is replaced by an equivalent (from the viewpoint of the magnetic field outside the sphere) system "coil - imaginary coil". The balance of the flux variations includes the decrease of the flux due to the exclusion of the field by the plasma $\Delta\Phi = \Phi_0 X^3$ and the contribution of the mutual inductance M_- of the coil current and its image. This total effect of the flux decrease should be compensated by its increase due to the pickup coil with current J and inductance L_0.

Then the relation for determining the pickup coil current is given as follows [10]

$$J(X) = \frac{J_{0,max} X^3}{1 - KX^3}, \tag{5.3}$$

where $J_{0,max} = \dfrac{\Phi_0}{L_0}$. The total initial flux Φ_0 is given as $\Phi_0 = \pi R_c^2 B_0$, where B_0 is the uniform initial magnetic field.

The corresponding real inductive energy of the coil with the maximum current J_{max} is equal to

$$W_{max} = \frac{1}{2} L J_{max}^2. \tag{5.4}$$

The part 2.3 in Fig. 5.5 "Calculation of the pickup coil magnetic field" calculates the magnetic field of the coil $\vec{B}_c$ due to the current in the coil.

The total magnetic field $\vec{B}$ is calculated as follows.

$$\vec{B} = \vec{B}_0 + \vec{B}_p + \vec{B}_c,$$

where $\vec{B}_p$ is the magnetic field of plasma and $\vec{B}_c$ is the magnetic field of pickup coil.

For finding the plasma magnetic field $\vec{B}_p$, Faraday's law

$$\frac{\partial \vec{B}_p}{\partial t} = -\nabla \times \vec{E} \tag{5.5}$$

is used, where $\vec{E}$ is the electrical field.

Differentiating the total magnetic field with taking into account that the initial magnetic field $\vec{B}_0$ does not depend on time and Faraday's law (5.5), we carry out that

$$\frac{\partial \vec{B}}{\partial t} = \frac{\partial \left(\vec{B}_0 + \vec{B}_p + \vec{B}_c\right)}{\partial t} = \frac{\partial \vec{B}_p}{\partial t} + \frac{\partial \vec{B}_c}{\partial t} = -\nabla \times \vec{E} + \frac{\partial \vec{B}_c}{\partial t}.$$

The finite - difference version of the last equation is written as follows:

$$\frac{\vec{B}^{\,m+\frac{1}{2}} - \vec{B}^{\,m-\frac{1}{2}}}{\Delta t} = -\left(\nabla \times \vec{E}^{\,m}\right)_h + \frac{\vec{B}_c^{\,m+\frac{1}{2}} - \vec{B}_c^{\,m-\frac{1}{2}}}{\Delta t},$$

where m is the number of time step and h indicates that finite - difference version of the term is considered. From the equation the magnetic field at next time step $\vec{B}^{\,m+\frac{1}{2}}$ can be written as follows:

$$\vec{B}^{\,m+\frac{1}{2}} = \vec{B}^{\,m-\frac{1}{2}} + \left(-\nabla \times \vec{E}^{\,m}\right)_h \Delta t + \vec{B}_c^{\,m+\frac{1}{2}} - \vec{B}_c^{\,m-\frac{1}{2}}.$$

In the pickup coil subroutine the difference $\vec{B_c}^{m+\frac{1}{2}} - \vec{B_c}^{m-\frac{1}{2}}$ is calculated and then the difference is added to the total magnetic field.

For the code modification according to the problem we added the coil current $\vec{J}$ to the equation for the electric field $\vec{E}$.

$\vec{B}_c$ is evaluated from the equation:

$$\nabla \times \vec{B}_c = \mu_0 \vec{J}.$$

The equation for $\vec{E}$ that takes into account the pickup coil current is evaluated as follows

$$\vec{E} = \frac{1}{Zen_i}\left\{\frac{1}{\mu_0}\left(\nabla \times \vec{B}\right) \times \vec{B} - \vec{J_i} \times \vec{B} - ZT_e \nabla n_i\right\} -$$
$$-\frac{1}{Zen_i\mu_0}\left\{\left(\nabla \times \vec{B}_0\right) \times \vec{B}\right\} - \frac{1}{Zen_i}\vec{J} \times \vec{B},$$

where n_i is the ion number density, $Zn_i = n_e$, n_e the electron number density, e the elementary electric charge, $\vec{J_i}$ the ion current density, T_e the electron temperature and it is assumed to be uniform for simplicity. $\vec{J}$ is the pickup coil current.

This formulation is self - consistent. The third term of the equation is the correction term for the pickup coil calculation.

For each component of vector $\vec{E} = (EX, EY, EZ)$ the equation can be rewrite as follows.

$$EX = \frac{1}{Zen_i}\left\{\frac{1}{\mu_0}\left(\left(\frac{\partial BX}{\partial z} - \frac{\partial BZ}{\partial x}\right)BZ - \left(\frac{\partial BY}{\partial x} - \frac{\partial BX}{\partial y}\right)BY\right) -\right.$$
$$\left. - (JY_iBZ - JZ_iBY) - ZT_e\frac{\partial n_i}{\partial x}\right\} -$$
$$\frac{1}{Zen_i\mu_0}\left\{\left(\frac{\partial BX_0}{\partial z} - \frac{\partial BZ_0}{\partial x}\right)BZ - \left(\frac{\partial BY_0}{\partial x} - \frac{\partial BX_0}{\partial y}\right)BY\right\} - \frac{1}{Zen_i}JYBZ;$$
$$EY = \frac{1}{Zen_i}\left\{\frac{1}{\mu_0}\left(\left(\frac{\partial BY}{\partial x} - \frac{\partial BX}{\partial y}\right)BX - \left(\frac{\partial BZ}{\partial y} - \frac{\partial BY}{\partial z}\right)BZ\right) -\right.$$
$$\left. - (JZ_iBX - JX_iBZ) - ZT_e\frac{\partial n_i}{\partial y}\right\} -$$
$$\frac{1}{Zen_i\mu_0}\left\{\left(\frac{\partial BY_0}{\partial x} - \frac{\partial BX_0}{\partial y}\right)BX - \left(\frac{\partial BZ_0}{\partial y} - \frac{\partial BY_0}{\partial z}\right)BZ\right\} + \frac{1}{Zen_i}JXBZ;$$

$$EZ = \frac{1}{Zen_i}\left\{\frac{1}{\mu_0}\left(\left(\frac{\partial BZ}{\partial y} - \frac{\partial BY}{\partial z}\right)BY - \left(\frac{\partial BX}{\partial z} - \frac{\partial BZ}{\partial x}\right)BX\right) - \right.$$

$$\left. - (JX_i BY - JY_i BX) - ZT_e\frac{\partial n_i}{\partial z}\right\} -$$

$$\frac{1}{Zen_i\mu_0}\left\{\left(\frac{\partial BZ_0}{\partial y} - \frac{\partial BY_0}{\partial z}\right)BY - \left(\frac{\partial BX_0}{\partial z} - \frac{\partial BZ_0}{\partial x}\right)BX\right\} - \frac{1}{Zen_i}(JXBY - JYBX).$$

Then we move to the finite-difference equations. For instance, finite-difference equation for X component of electric field is given as follows.

$$EX(i,j,k) = \frac{1}{Zen_i}\left\{\frac{1}{\mu_0}\left(\left(\frac{BX(i,j,k+1) - BX(i,j,k-1)}{2\Delta z} - \right.\right.\right.$$

$$\left.\left.\left. - \frac{BZ(i+1,j,k) - BZ(i-1,j,k)}{2\Delta x}\right)BZ(i,j,k) - \right.\right.$$

$$\left.\left. - \left(\frac{BY(i+1,j,k) - BY(i-1,j,k)}{2\Delta x} - \frac{BX(i,j+1,k) - BX(i,j-1,k)}{2\Delta y}\right)BY(i,j,k)\right) - \right.$$

$$\left. - (JY_i(i,j,k)BZ(i,j,k) - JZ_i(i,j,k)BY(i,j,k)) - ZT_e\frac{n_i(i+1,j,k) - n_i(i-1,j,k)}{2\Delta x}\right\} -$$

$$- \frac{1}{Zen_i\mu_0}\left\{\left(\frac{BX_0(i,j,k+1) - BX_0(i,j,k-1)}{2\Delta z} - \frac{BZ_0(i+1,j,k) - BZ_0(i-1,j,k)}{2\Delta x}\right)\times\right.$$

$$\times BZ(i,j,k) - \left(\frac{BY_0(i+1,j,k) - BY_0(i-1,j,k)}{2\Delta x} - \frac{BX_0(i,j+1,k) - BX_0(i,j-1,k)}{2\Delta y}\right)\times$$

$$\left.\times BY(i,j,k)\right\} - \frac{1}{Zen_i}JY(i,j,k)BZ(i,j,k).$$

The last term of the equation is a correction term for the electric field equation.

5.4 Results and discussion

In this section, we will present the simulation results along with discussion. The simulation results are compared with the data of simulative experiment "Generator" on quasi-spherical expansion of laser plasma into the magnetic field that was performed by Zakharov et al. [10], [11].

Calculations are performed for different values of parameter K ($K \approx 2/\ln G$ and $K \approx 3.6/\ln G$) since its variation is connected with some uncertainties concerning the coil shape and the best fitting to experimental relation of pickup coil current J. Taking into account the error of experimental measurements, we have also varied the plasma mass and plasma energy. The common calculation parameters and the variation parameters are shown in Tables 5.1 and 5.2, respectively. In Table 5.2, values for cases 2 and 5 (nominal cases) are estimated from the experiment.

Table 5.1. Common calculation parameters.

pickup coil radius R_c $[m]$	0.075
cross section radius of pickup coil r_c $[m]$	0.003
pickup coil inductance L_0 $[nH]$	310
initial plasma radius R_p $[m]$	0.0051
atomic mass $[amu]$	6.5
effective charge Z	2.5
magnetic field B_0 $[T]$	0.062
cyclotron frequency ω_c $[sec^{-1}]$	2.28×10^6
time step $[ns]$	0.438
calculation region $[m]$	$0.15 \times 0.15 \times 0.25$
mesh size	$30 \times 30 \times 50$
number of particles simulated	100000

Table 5.2. Variation parameters.

K	Case	mass $[mg]$	energy $[J]$
$3.6/\ln G$	1	1	10.4
	2*	1.5	8
	3	2	5.6
$2.0/\ln G$	4	1	10.4
	5*	1.5	8
	6	2	5.6

* Nominal case.

Magnetic field distributions along X axis are shown in Fig. 5.7 for Case 5. From the figure we can see that the magnetic field is excluded and the diamagnetic cavity is formed, the maximum value of the cavity reaching around $0.8\mu s$. The magnetic field is compressed between the diamagnetic cavity and the pickup coil, resulting in two peaks.

The simulation results for the time evolutions of particle position are shown in Fig. 5.8 for Case 5, where they are projected onto the XZ plane. As we can see in these figures, the plasma shape is spherical at the initial stage and then the particles are retardated by the magnetic field, especially at the pickup coil region and its shape changes to follow the magnetic field line. From the picture at $1.4\mu s$ we can see that the plasma particles are ejected from the coil region.

Figures 5.9 (a) and (b) present a comparison between experimental and simulation results of particle distribution in XY plane. The asymmetrical shape of the plasma expansion in the experiment is related with the laser beam paths which correspond to the preferable directions of the plasma expansion (right and left). In the experimental result we can see the flute instability, but we did not observe the instability in the simulation results.

In our simulation we omitted the term of field's diffusion due to the instability in the equation of electron fluid and we also assumed that the plasma expansion is

isotropic at the initial stage. The facts make difficult the comparison and partly explain the differences.

Figures 5.10 (a) and (b) show the simulation results for dependences of pickup coil current on time for different values of parameter K, plasma mass and plasma energy. The curve of Case 2 in Fig. 5.10 (a) corresponds to the experimental parameters for $K = 3.6/\ln G$. In that case the maximum value of the pickup coil current is about $2900A$ that reaches at $0.7\mu s$. On the other hand from the experiment curve we can see that the maximum current is about $1875A$ at $0.75\mu s$. Case 1 curve in Fig. 5.10 (a) reaches a relatively high value of the maximum coil current ($3100A$) at early time (about $0.5\mu s$). The maximum value of the current in Case 3 is about $2500A$ at $0.9\mu s$.

Case 5 curve (see Fig. 5.10 (b)) corresponds to the results for the other value of $K = 2.0/\ln G$ and the maximum current is $2400A$ at $0.8\mu s$. The maximum coil currents of the last two curves Case 4 and 6 are $2500A$ and $2200A$ at $\sim 0.52\mu s$ and $\sim 1.15\mu s$ respectively.

From the fact that the maximum cavity radius reaches when the coil current reaches the maximum value, we can conclude that from the nominal Cases 2 and 5 of simulation the maximum cavity radius reaches at $0.7\mu s$ (Case 2) and at $0.8\mu s$ (Cases 5). The cavity radius is preserved during about $0.5\mu s$, after that time the cavity begin to collapse. On the other hand, from the experimental curves it was found that the cavity radius stays near its maximal value during the time about $0.3\mu s$ (slightly after $t = 1\mu s$).

In addition, the dotted - dashed curves indicate the experiment error. As reported in Ref. [11], for the pickup coil current J, the error is about $\pm 15\%$. Even if we take into account the experimental error the difference between our simulation data and experiment one is at least $+7 \sim 9\%$. In other words, we can not explain the difference due to the experimental error.

The main differences between experiment results and simulation ones are as fol-

lows. In the experiment the cavity collapses rapidly after its maximum value due to development of the flute instability ([20], [21]) as seen in Fig. 5.9 (a), while the instability did not develop in the simulation.

The numerical results for field variation inside the coil (5 cm from the coil center) are shown with the experimental results in Figs. 5.11 (a) and (b). The maximum values of ΔB ($\Delta B = B - B_0$) of the curves correspond to magnetic field compression between the pickup coil and diamagnetic cavity (at this stage the observation point is outside of the diamagnetic cavity). After approximately $0.35\mu s$ (see Fig. 5.7) we can observe that the magnetic field is excluded ($B < B_0$) from the observation point by the plasma particles and the observation point locates in the cavity.

The values of field exclusion for the simulation data (Cases 1 — 6) are large than that of the experiment data (solid line in Figs. 5.11 (a) and (b)). On the other hand, according to the simulation data the time of field exclusion is longer than in the experiment.

As before, together with the experimental curve we consider the error ones. The error for ΔB is approximately $\pm 15\%$ and the reason of difference between the experimental and simulation results is not the experimental error.

Figure 5.12 shows the dependences of diamagnetic cavity radius on time that were obtained from simulation. The results confirm the previous ones (see Fig. 5.10): the maximum cavity radius depends on K and reaches slightly after $\sim 0.7\mu s$ (Cases 2) and $\sim 0.8\mu s$ (Cases 5). The cavity begins to collapse gently.

Figures 5.13 (a) and (b) show the magnetic flux change e_r given by $e_r = 100 \cdot (\Phi - \Phi_0)/\Phi_0$, where Φ_0 is the initial magnetic flux. From the figure we can conclude that for nominal Cases 2 and 5 the magnetic flux is conserved within 15% and 10%, respectively.

The dependence of the dimensionless gap size δ between the coil and diamagnetic cavity ($\delta = (R_c - R_{cav}^{max})/R_c$) on the main similarity criterion of the problem $\beta = R_c/R_b$ is shown in Fig. 5.14. Dashed line is the theoretical dependence that was

obtained in Ref. [10]. The squares are simulation results of Cases 1 - 3 and the circles are simulation results of Cases 4 - 6. From the figure we can see a good agreement between simulation results and theoretical one for $0.5 \leq \beta \leq 1$. However the results from Cases 4 — 6 correspond to the theoretical line better.

We can conclude that a qualitative agreement between the simulation and experimental data was found. Cases 4 — 6, especially Case 5, for $K = 2.0/\ln G$ reproduce the experiment data better (see Figs. 5.10, 5.11, 5.12 and 5.14). The good agreement was found for the dependence of the gap size δ on the similarity criterion β (see Fig. 5.14).

The experimental value of conversion efficiency is $4.5 \pm 0.9\%$ that corresponds to the maximum pickup coil current of $1875A$, however from our result (Case 5) the efficiency is estimated to be 7.9% for the current of $2400A$ by using the equation $W_{max} = L_c J_{max}^2/2$. For the estimation of conversion efficiency η we use the ideal equation as follows.

$$\eta = \frac{W_{max}}{E_0}. \tag{5.6}$$

It is very important to reproduce the maximum coil current J_{max}, because the efficiency η is proportional to J_{max}^2.

5.5 Conclusions

For a direct energy conversion process, a pickup coil that encloses the expanding diamagnetic plasma cloud is used [1]. To simulate the real process of direct energy conversion, "Generator" experiment was conducted by Zakharov et al. [10] at $KI-1$ facility. The dynamics of the pickup coil current, field exclusion inside the coil and the dynamics of plasma expansion were examined and a conversion efficiency was estimated.

For comparative purposes we performed numerical analysis on plasma behaviors in the magnetic field in the presence of the pickup coil and took into account the mutual inductance of the plasma cloud and the coil. The numerical analysis was performed by using a $3D$ hybrid PIC code.

In general we had obtained a reasonable accordance between the experiment and $PIC-$ simulation results especially on the dependence of the dimensionless gap size δ between the diamagnetic cavity and the pickup coil on the main similarity criterion of the problem β (see Fig. 5.14).

According to Ref. [10] the experimental value of conversion efficiency η is $4.5 \pm 0.9\%$ that corresponds to the maximum pickup coil current of $1875A$, however from the our results (Case 5, Section **5.4**) the efficiency is estimated to be 7.9% for the current of $2400A$. In our simulation we omitted the term of field's diffusion (due to the instability) in the equation of electron fluid and we also assumed that the plasma expansion is isotropically at the initial stage. On the other hand, the instability is occurring and two - side illumination of the target (asymmetrical expansion of initial plasma) is used in the experiment. Probably, these reasons determine the differences between the simulation and experiment results.

References

[1] ARTSIMOVICH L.A.: "Controlled Fusion Reactions", *Chapter 1.2, Direct Conversion of Fusion Energy into Electric one, Physics & Mathematics, Moscow* (1963), (in Russian)

[2] HAUGHT A.F., POLK D.H. AND FADER W.J.: *Phys. Fluids,* **13** (1970) 2842.

[3] HYDE R., WOOD L. AND NUCKOLLS J.: *AIAA Paper, New York, N* 72-1063 (1972) 312.

[4] LEVIN M.L.: *Sov. Phys. Technic. Phys.,* **9** *N* 3 (1964) 312.

[5] BELOOZEROV V.N.: *Soviet Physics — Technical Physics,* **11** *N* 5 (1966) 631.

[6] MIMA K., YOSHIKAWA K., MORIMIYA O., TAKASE H., TAKABE H., KITAGAWA Y., TAJIMA T., KOSAKI Y. AND NAKAI S.: *Fusion Technology,* **22** (1992) 56

[7] NAKASHIMA H., TAKADA M. AND KANDA Y.: *Fusion Engineering and Design, North - Holland, Elseiver Science Publeshers B.V.,* **15** (1992) 255.

[8] DICKMAN D.O. ET AL.: *Phys. Fluids,* **12** (1969) 1708.

[9] SHOYAMA H., NAKASHIMA H. AND KANDA Y.: *J. of Plasma and Fusion Research,* **69** *N* 10 (1993) 1250.

[10] ZAKHAROV YU.P., MELIKHOV A.V., POSUKH V.G. AND SHAIKHISLAMOV I.F.: *J. of Appl. Mech. and Technic. Phys.,* **42** *N* 2 (2001) 185.

[11] ZAKHAROV YU.P. AND NAKASHIMA H.: *Proc. 11 Int. Conf. Emerging Nuclear Energy Systems, Dan Knassim Ltd., Ramat Gan, Israel,* **1** (2002) 319.

[12] WINTERBERG F.: *Raumfahrtforschung,* **15** (1971) 208.

[13] WOOD L. AND WEAVER T.: *UCID - 16229* (1973).

[14] BURK R.J. AND CUTTING J.C.: *Proc. 1st ANS Topl. Mtg. Tech. of Controlled Nuclear Fusion,* (1974) 53.

[15] TSUJI R. AND IDO S.: *Jpn. J. Appl. Phys.,* **22** (1983) 987.

[16] LASCHE G.P.: *UCRL - 53434* (1983).

[17] ZAKHAROV YU.P., PONOMARENKO A.G., NAKASHIMA H., ET AL.: *Proc. of the 9th Int. Conf. on Emerging Nuclear Energy System,* (Herzlia, June 28 - July 2, 1998), **1**, Dan Knassim Ltd., Romat - Gan, (1998) 384.

[18] SUDO S., SATO K., AND SEKIGUCHI T.: *J. Phys. D: Appl. Phys.,* **11** (1978) 389.

[19] ZAKHAROV YU.P., ANTONOV V.M. AND MELIKHOV A.V.: *AIP Conf. Proc.,* 369 (1996) 357.

[20] OKADA S., SATO K. AND SEKIGUCHI T.: *J. Phys. Soc. Jpn.,* **46** No.1 (1979) 355.

[21] ZAKHAROV YU.P., ORISHICH A.M., PONOMARENKO A.G. AND POSUKH V.G.: *Sov. J. Plasma Phys.,* **12** (1986) 674.

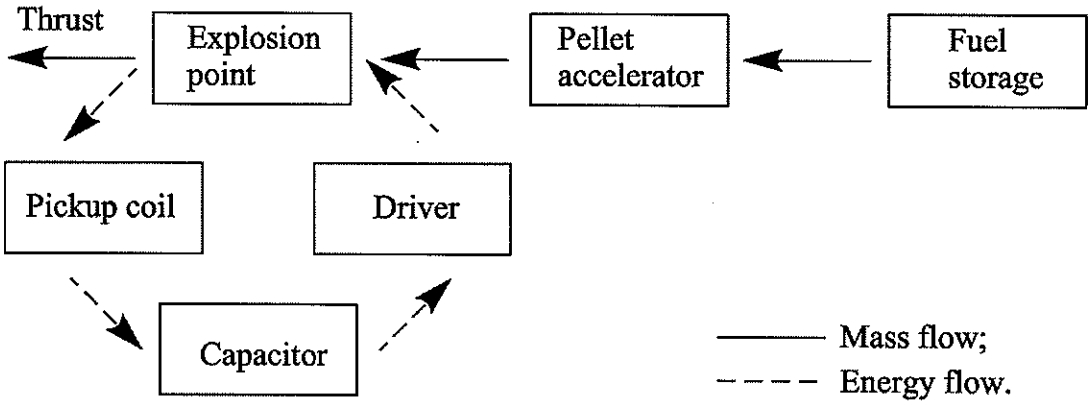

Fig. 5.1 Mass and energy flow diagram.

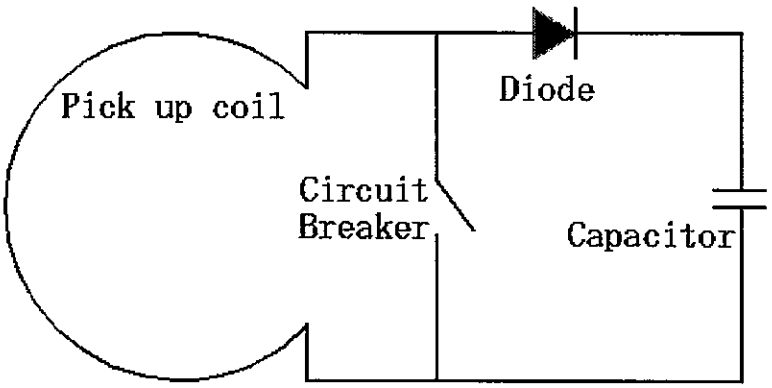

Fig. 5.2 Energy recovery circuit that uses a capacitor load with diode.

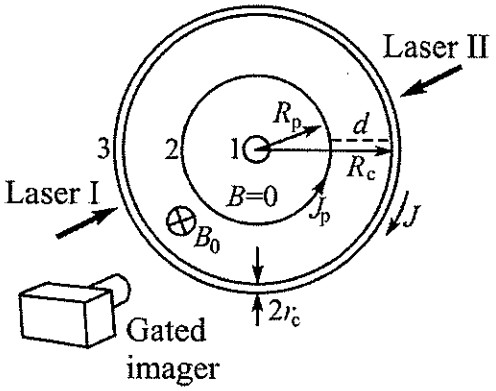

Fig. 5.3 Schematic of "Generator" experiment.

1 spherical pellet target; 2 plasma cloud; 3 pickup coil.

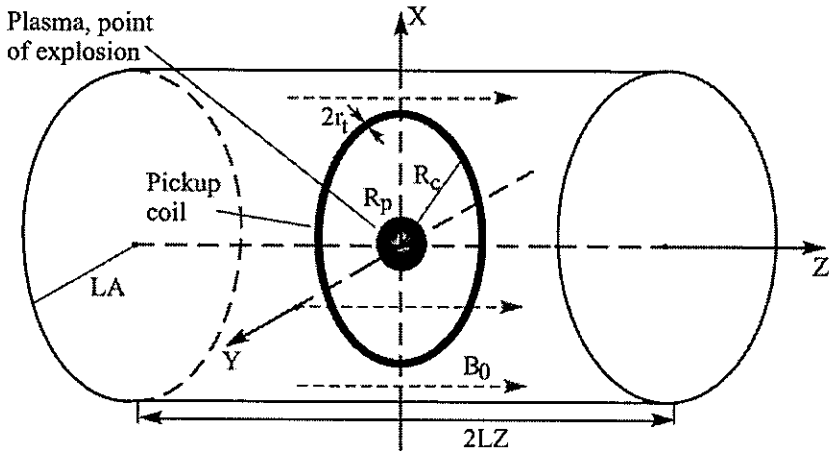

Fig. 5.4 Calculation model.

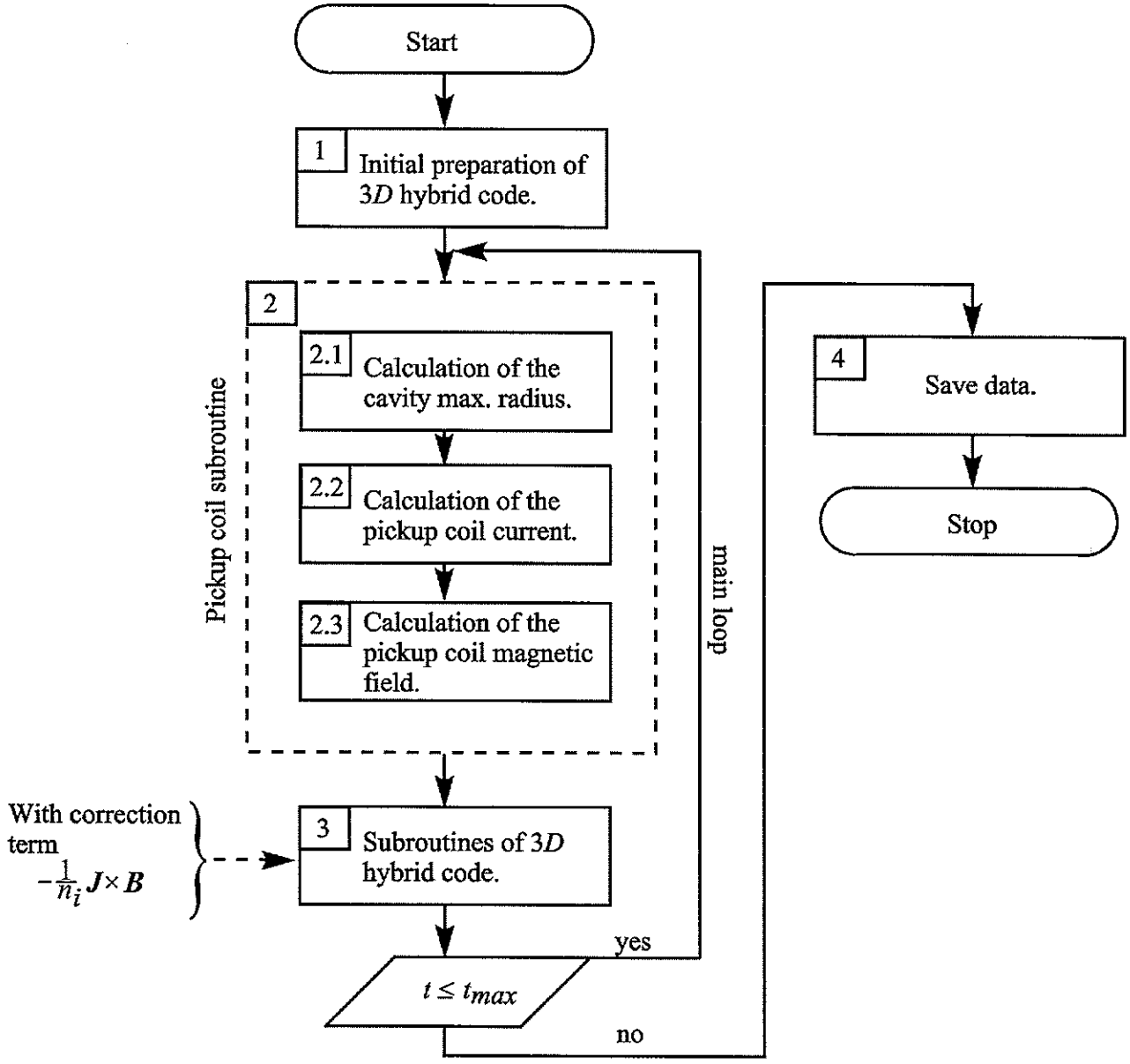

Fig. 5.5 Flow chart of pickup coil subroutine.

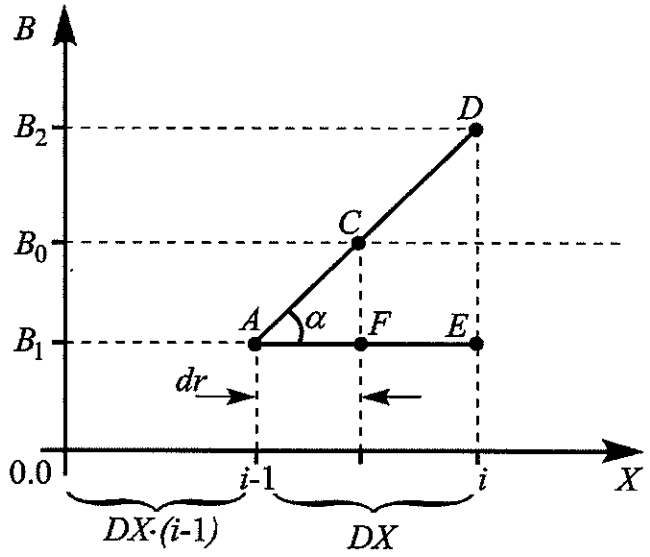

Fig. 5.6 Calculation of the maximum cavity radius.

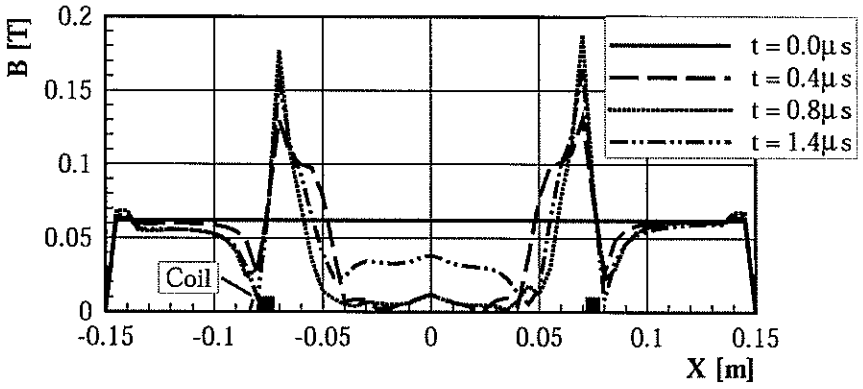

Fig. 5.7 Magnetic field along X - axis.

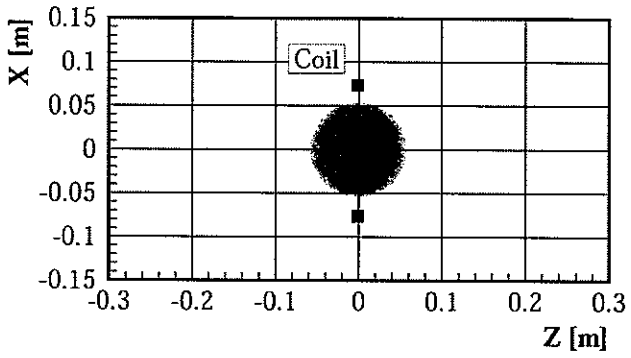

$t = 0.4\mu s$

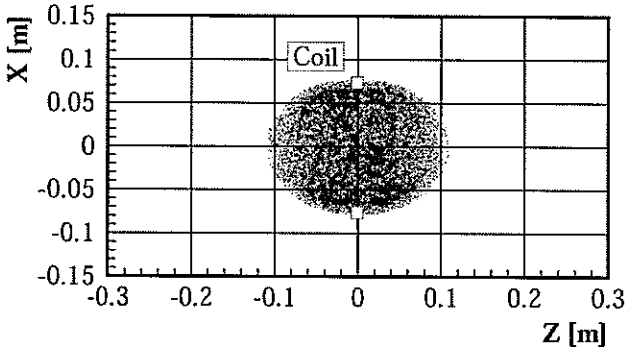

$t = 0.8\mu s$

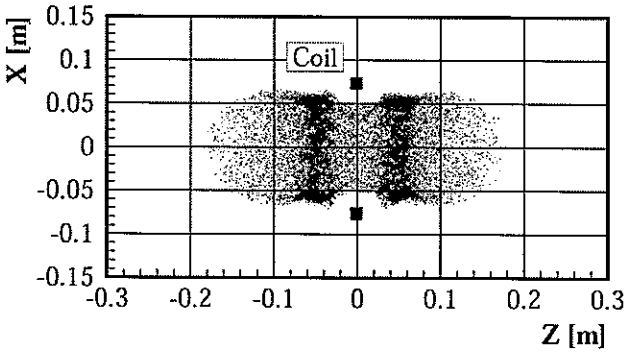

$t = 1.4\mu s$

Fig. 5.8 Particle distribution projected onto ZX - plane (Case 5).

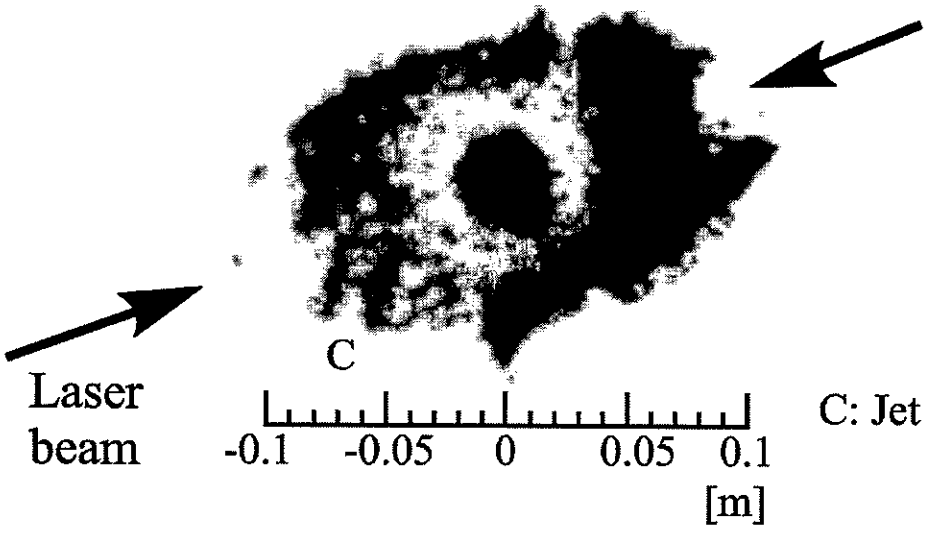

(a)

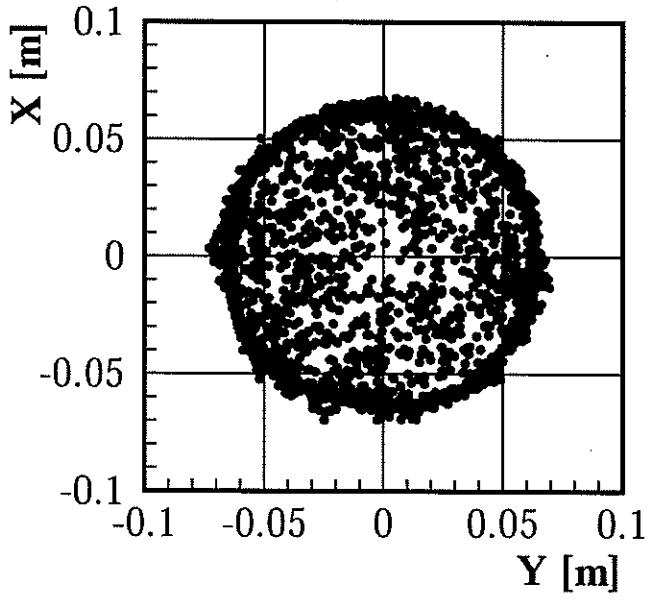

(b)

Fig. 5.9 Comparison of particle positions between (a) experiment (top) and (b) simulation (bottom) at $1\mu s$.

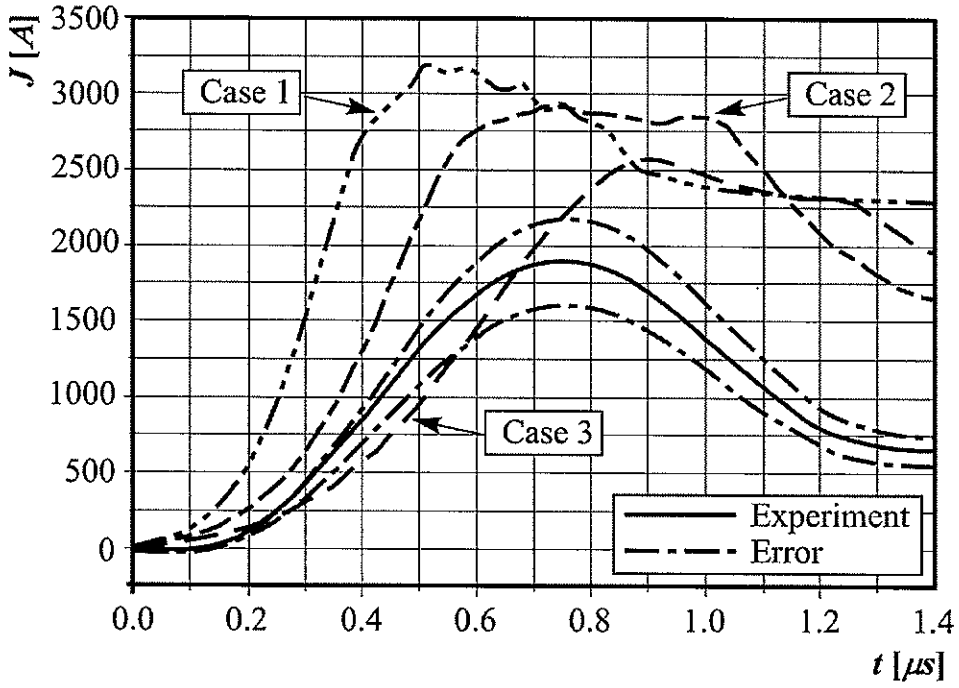

(a)

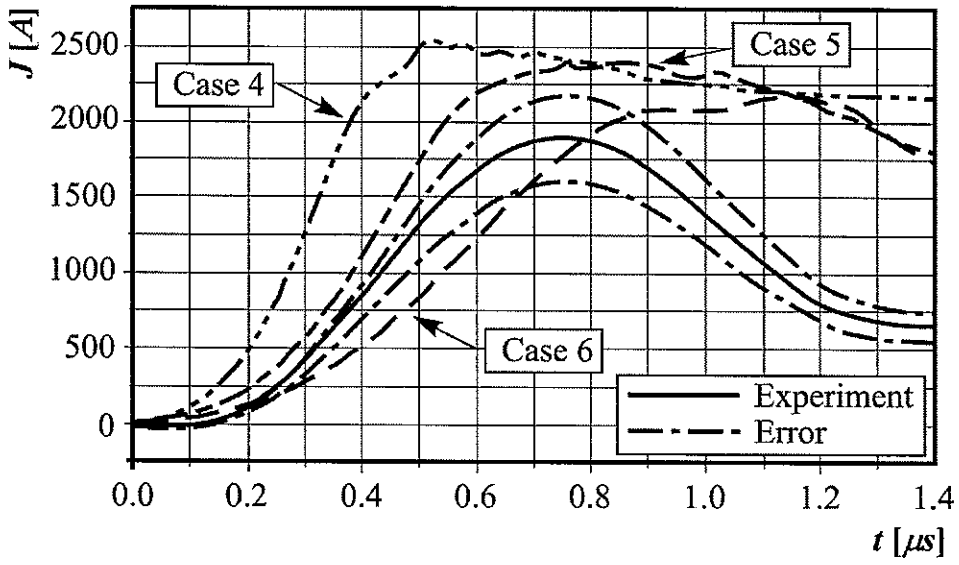

(b)

Fig. 5.10 Dynamics of the current (a) $K = 3.6/\ln G$, (b) $K = 2.0/\ln G$.

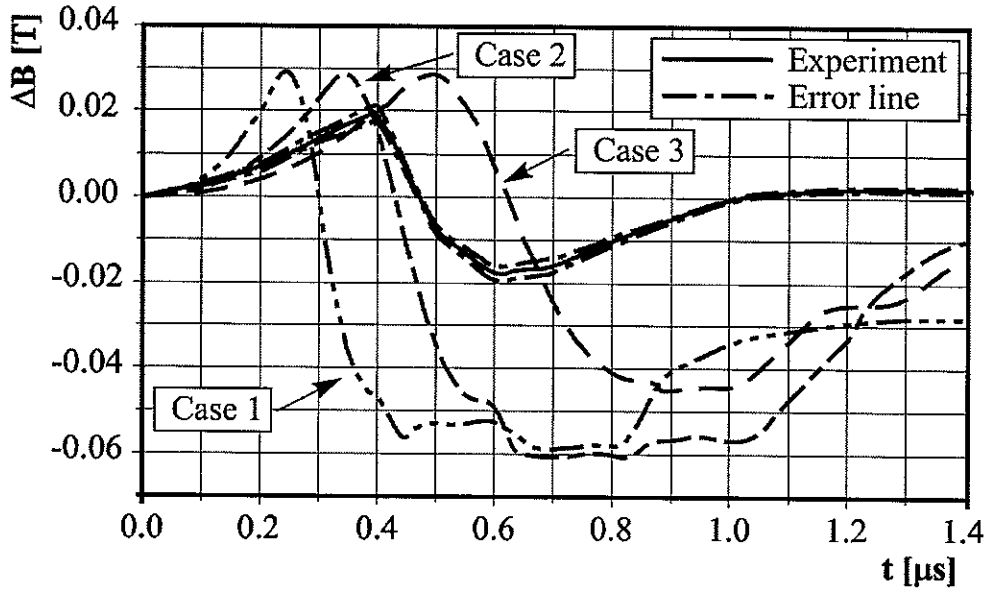

(a)

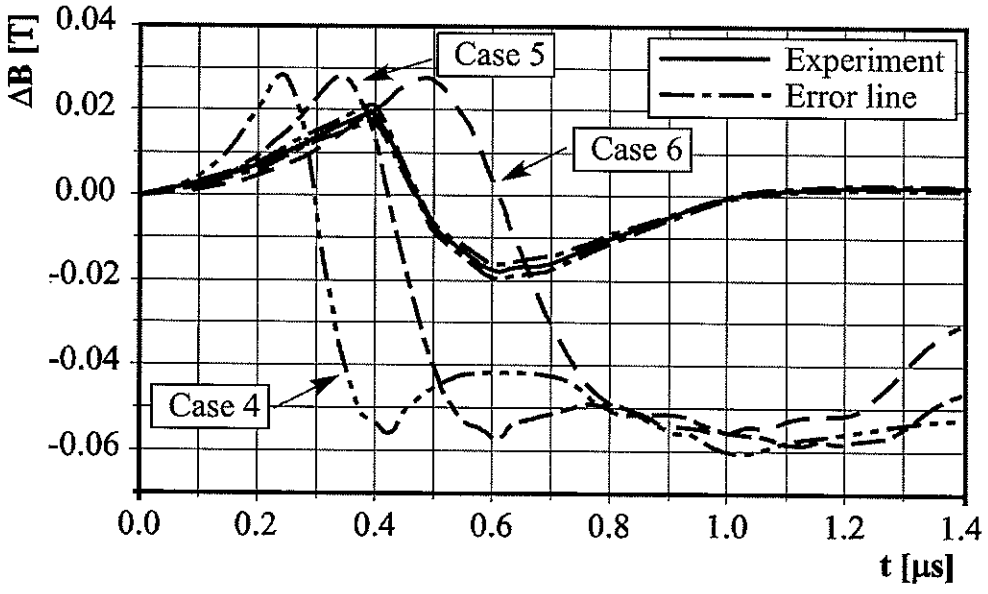

(b)

Fig. 5.11 Difference of the magnetic field (a) $K = 3.6/\ln G$, (b) $K = 2.0/\ln G$.

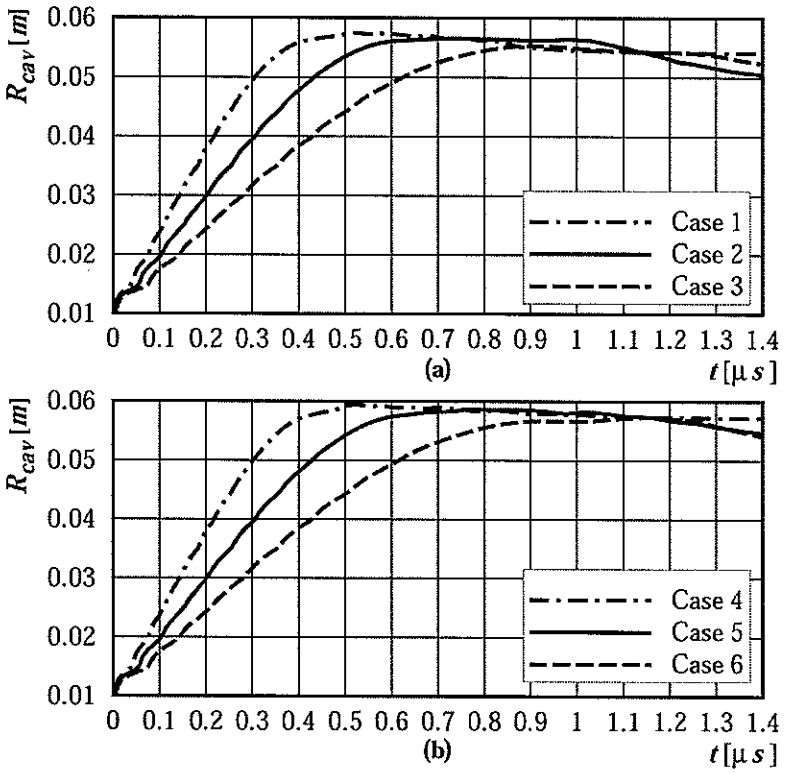

Fig. 5.12 Variation of diamagnetic cavity radius with time (simulation result).

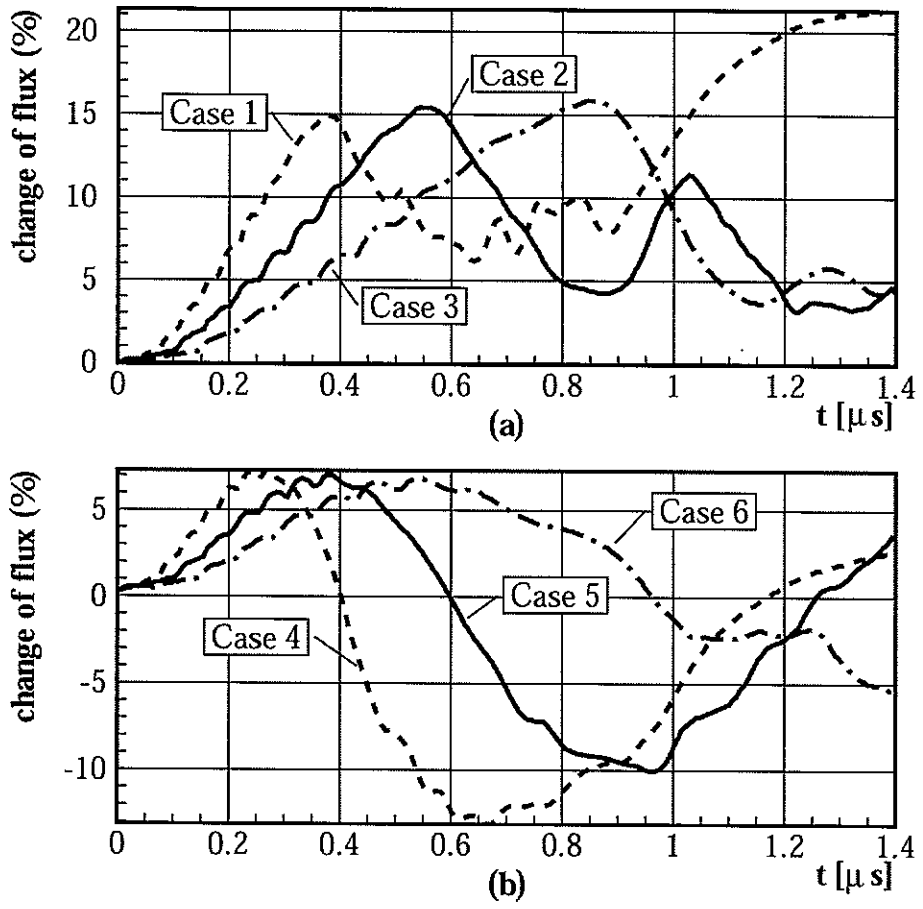

Fig. 5.13 Magnetic flux change (a) $K = 3.6/\ln G$, (b) $K = 2.0/\ln G$.

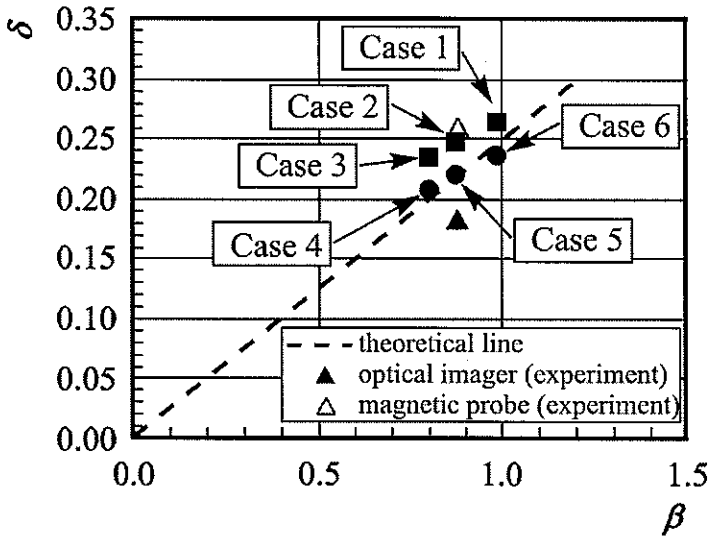

Fig. 5.14 The dependence of the dimensionless gap size δ on the main similarity criterion β.

6 Conclusions

This chapter gives an overview of the main conclusions of this work and suggestions for the further work.

The main goal of this study has been investigation of thrust conversion process of explosive plasma source in dipole magnetic field by using the $3D$ hybrid PIC code. It involves the following problems.

1. Comparison analysis of laser - produced plasma experiment and simulation study;
2. Optimization of thrust efficiency;
3. Direct conversion of plasma cloud energy into electrical energy.

The work is crucial for understanding the physics phenomena that occur in the magnetic thrust chamber using the dipole magnetic field, as well as for designing an optimal configuration of the chamber for laser thermal propulsion as well as inertial confinement fusion rockets.

To calculate the plasma behavior under the dipole magnetic field in the chamber, the $3D$ hybrid PIC code is applied. The hybrid code treats ions as individual particles and electrons as a fluid.

For the first problem we use the results of "Impulse" experiment performed at $KI-1$ facility. In the experiment, the real processes of plasma momentum transfer in a dipole - like magnetic field is simulated and the thrust conversion efficiency is determined.

The results of the work are as follows.

1. It has been shown that at the early time, the plasma expands isotropically, and then the shape of the plasma changes to follow the dipole magnetic field line.
2. A qualitative agreement between experimental and simulation results is found for the time evolutions of particles positions and the magnetic field disturbances

ΔB caused by the diamagnetic cavity of plasma.

3. From the comparison analysis we could conclude that a thrust conversion efficiency as high as 60% is possible in the scaled - down model of the thrust chamber considered here.

For optimization of the thrust conversion efficiency, the time - integrated picture of exploding plasma movement in the thrust chamber is examined. The comparison analysis is performed between simulation and MHD - Nikitin model which is dedicated to find the configuration of the plasma front as a function of time and the limits of its propagation. Calculations are performed for several cases with the different values of energetic parameter κ.

The results of the work are as follows.

1. The time - integrated picture of plasma cloud shows a cone - like geometry and the half angle of the plasma expansion cone α is estimated. It also is shown that $\alpha = 50°$ in the optimum case.

2. Overall qualitative agreement is found between the simulation and the theoretical model of Nikitin for dependences of the thrust efficiency η on α and κ.

3. Simulation results show the maximum thrust efficiency is about 70%, however in the MHD theoretical work the efficiency reaches about 85%.

For the investigation of conversion process of initial kinetic energy of plasma cloud into electrical energy we are comparing the efficiency of such conversion process between experiment and simulation. Some of the kinetic energy should be picked up to provide the electric energy for drivers. The direct energy conversion is realized due to inductive generation of currents in a pickup coil that encloses the plasma and is oriented across the external magnetic field.

For the comparative purpose we use the results of "Generator" experiment performed at the $KI-1$ facility. The experiment simulates the real processes of direct conversion to determine the conversion efficiency.

The results of the work are as follows.

1. It has been shown that the magnetic field is compressed between the diamagnetic cavity and the pickup coil and the current is generated in the pickup coil. It is also shown that the plasma particles are ejected from the coil region by the magnetic field of the pickup coil.

2. In the experimental result there is the flute instability, but we do not observe the instability in the simulation results. In our simulation we have omitted the term of field's diffusion and we have also assumed that the plasma expansion is isotropic at the initial stage. The facts make difficult the comparison and partly explain the differences.

3. A reasonable agreement is found for dependence of the gap size δ on the similarity criterion of the problem β.

4. The experimental value of conversion efficiency is $4.5 \pm 0.9\%$, while from the simulation results the efficiency is estimated to be 7.9%. To decrease the difference, more sophisticated model with the instability term is required for the model of induced pickup coil current.

In summary, we have developed a $3D$ hybrid code and we have also analyzed the behaviors of the plasma expansion in the magnetic thrust chamber using dipole magnetic field. From comparative analysis between the simulation and experiment, it is found that the $3D$ hybrid code developed here simulates properly the behaviors, thus indicating that this code is applicable to the thrust chamber design. By using the code, optimization of the thrust conversion efficiency is conducted for the magnetic thrust chamber and the maximum level of thrust efficiency up to 70% is estimated in an optimum configuration of the thrust chamber. So, this level of

thrust efficiency could be obtained in the magnetic thrust chamber. These results would substantiate the idea of direct and highly effective usage of explosive plasma sources in the form of magnetic thrust chamber for propulsion purposes.

Our suggestions for the further work are as follows:

1. In future, large - scale simulative experiments should be performed for study of magnetic thrust chamber design; for instance, experiments with uniform irradiation of target should be conducted.

2. Make a calculation with the instability term in the direct energy conversion.

3. Adapt the code for the calculation on the supercomputers with multiprocessors.

Appendix

The direct determination of dipole momentum P_d via magnetic field disturbances b_θ and dipole field B_ρ was described by Zakharov et al. Ref. [26] (Chapter 3). The determination of P_d is based on the new method of magnetic probe measurements of the volume force $F_z^p \propto J_\varphi B_\rho$ arising in the surface S of the shell housing of dipole μ_d (with its own field B_ρ at S, see Fig. A1) when the plasma diamagnetic cavity appears, and the skin current J_φ should be generated to exclude from the conductive housing the magnetic field b_θ (of plasma moment μ_c). More strictly speaking, this b_θ field is the sum of the field of plasma moment μ_c and the field of its "image" inside the shell, with the moment $\mu_{ci} = \gamma^3 \mu_c$ shifted from the shell center toward μ_c to the distance γR_S (where the additional similarity criterion of the problem of the "shielded dipole" is $\gamma = R_S/R_0$, R_S being the dipole shell radius and R_0 the point of injection). In the case of very thin skin - layer of J_φ, the volume integration of its ponderomotive force $F_z^p = J_\varphi B_\rho$ could be replaced (using Maxwell tensor) by the surface one and a very useful relation for measuring the dipole impulse could be obtained as follows:

$$P_d = \frac{1}{\mu_0} \int dt \int b_\theta B_\rho dS \equiv \int F_z^p dt.$$

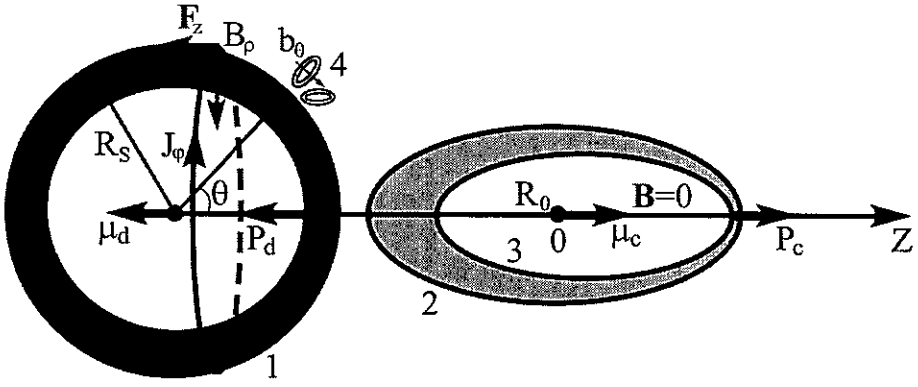

Fig. A1 General scheme of "Impulse" experiment. 1 dipole's shell; 2 plasma cloud; 3 diamagnetic cavity of LPC, 4 magnetic probes at dipole shell to determine its impulse P_d via b_θ - measurements.

Acknowledgements

The research was conducted at the Advanced Energy Engineering Science (AEES) department of Kyushu University.

The author would like to acknowledge those who gave generously their time, experience and resources to help the author in his study. First of all, the author would like to thank his advisor, Prof. Hideki Nakashima, for scientific guidance of the present work, his useful advices, critical reading of the manuscript, support and encouragement throughout of author's study. The author wishes to thank the reviewers, Prof. Kohnosuke Sato and Prof. Yasuyuki Nakao for the valuable comments and useful remarks to improve the manuscript. Also, the author owes Dr. Toshihiko Kawano for useful consultations regarding calculations on available powerful computers and Dr. Takanobu Muranaka for providing the source version of a calculation code.

The author is very grateful for the assistance to the following students of AEES department: Mr. Tomonori Esaki, Mr. Fumihiro Ichikawa and Mr. Daisaku Nakahara. Moreover, the author wishes to express his appreciation to entire staff of the department for various help and providing friendly warm-hearted support during the author's stay in Japan.

For fruitful discussions of the main results of this thesis and useful comments the author acknowledges to Dr. Yuri P. Zakharov (Institute of Laser Physics SD RAS), Dr. Segey A. Nikitin (Budker Institute of Nuclear Physics SD RAS), Prof. Galina I. Dudnikova (Institute of Computational Technologies SD RAS) and Prof. Vitali A. Vshivkov (Institute of Computational Mathematics and Mathematical Geophysics SD RAS). Dr. Yuri P. Zakharov also read and introduced clarity into the manuscript.

A financial support from Japanese Government afforded the author the great opportunity for study in Kyushu University.

Finally, the author kindly thanks his family for warm encouragement and understanding.